Scientia Pharmaceutica

ÖSTERREICHISCHE PHARMAZEUTISCHE GESELLSCHAFT

MDPI

Article

Metformin Improves Recognition Memory, Attenuates Neuronal Damage, and Reduces Cerebellar Amyloid-like Deposits in Female Diabetic Mice

Joan Poblano, Luis E. Cobos-Puc *, María del C. Rodríguez-Salazar and Hilda Aguayo-Morales *

Facultad de Ciencias Químicas, Universidad Autónoma de Coahuila, Boulevard Venustiano Carranza S/N Esq. con Ing. José Cárdenas Valdés, República Oriente, Saltillo 25280, Mexico; joanhernandezpoblan@uadec.edu.mx (J.P.); carmen_rodriguez@uadec.edu.mx (M.d.C.R.-S.)

* Correspondence: luis.cobos@uadec.edu.mx (L.E.C.-P.); aguayohilda@uadec.edu.mx (H.A.-M.); Tel.: +52-844-415-5752 (L.E.C.-P.); Fax: +52-844-415-9534 (L.E.C.-P.)

Abstract

Type 2 diabetes mellitus (T2DM) has been associated with cognitive impairment and an increased risk of dementia in women. This study examined the effects of subchronic metformin treatment on recognition memory and brain pathology in female diabetic mice. T2DM was induced by streptozotocin and nicotinamide injections. Then, the mice received metformin (50, 150, or 250 mg/kg) orally for 28 days. Recognition memory was assessed using the Novel Object Recognition Test (n = 72). Biochemical analyses of whole-brain homogenates evaluated insulin, tau, and insoluble Aβ_{42} (n = 4). Histological analyses evaluated neuronal damage and amyloid-like deposits in the hippocampal Cornu Ammonis 1 (CA1) region, cerebral cortex, and cerebellum (n = 4). The diabetic mice exhibited hyperglycemia, hyperinsulinemia, dyslipidemia, impaired recognition memory, and neuronal damage. Metformin reduced blood glucose levels and improved recognition memory. Metformin also normalized serum and brain insulin levels and reduced neuronal damage in the CA1 region, cortex, and cerebellum. Metformin reduced cerebellar Congo red-positive amyloid-like deposits and decreased insoluble Aβ_{42} levels in whole-brain homogenates. However, at 250 mg/kg, metformin increased total and phosphorylated tau levels. These results suggest that metformin mitigates recognition memory deficits, attenuates neuronal damage, and reduces cerebellar amyloid-like deposits in female mice.

Keywords: diabetes; female mice; recognition memory; metformin; amyloid-like deposits; cerebellum; insulin

Check for updates

Academic Editor: Antoni Camins Espuny

Received: 3 September 2026
Revised: 12 October 2026
Accepted: 19 October 2026
Published: 21 October 2026

Copyright: © 2026 by the authors. Published by MDPI on behalf of the Österreichische Pharmazeutische Gesellschaft. Licensee MDPI, Basel, Switzerland. This article is an open access article distributed under the terms and conditions of the Creative Commons Attribution (CC BY) license.

1. Introduction

Type 2 diabetes mellitus (T2DM) is one of the most significant public health challenges of the 21st century. Its global prevalence continues to rise, and it is associated with various systemic complications [1]. Beyond the well-established metabolic consequences such as cardiovascular disease, nephropathy, and retinopathy [2], a growing body of evidence links T2DM to impaired cognitive function and an increased risk of dementia, including Alzheimer's disease (AD) [3–5]. Diabetes-associated cognitive impairment (DACI) commonly manifests as memory impairment, slowed processing speed, and impaired executive function. These symptoms can severely impact patients' quality of life. The pathophysiological mechanism underlying DACI is multifactorial and complex. It involves an intricate

network of dysfunctions, including cerebral insulin resistance, oxidative stress, chronic inflammation, dyslipidemia, and alterations in amyloid protein homeostasis [6–8].

Insulin resistance, a hallmark of T2DM, affects more than just peripheral tissues. The brain is an insulin-sensitive organ where insulin plays a vital role in synaptic plasticity, neuronal energy metabolism regulation, and cell survival [5]. Impaired insulin signaling in the central nervous system (CNS) disrupts these processes and creates an environment conducive to neurodegeneration. Meanwhile, T2DM promotes dyslipidemia, which is characterized by elevated circulating cholesterol levels [9]. Although the brain synthesizes its own cholesterol, evidence suggests that peripheral hypercholesterolemia can affect the integrity of the blood–brain barrier (BBB) [10]. This can contribute to brain pathology, including the accumulation of β-amyloid (Aβ) peptides. The aggregation and deposition of Aβ in the form of senile plaques is a fundamental neuropathological feature of AD [11–13]. Most studies examining neurodegeneration related to diabetes have focused on the hippocampus and cerebral cortex [14–16]. The Cornu Ammonis 1 (CA1) region of the hippocampus is particularly susceptible to metabolic and oxidative stress. Structural alterations in this area are closely associated with memory impairment [17]. However, comparatively little attention has been given to other brain regions that may also contribute to cognitive dysfunction. In this context, the cerebellum has emerged as a structure that may be involved in cognitive and affective processes, in addition to its traditional role in motor control. Anatomically, the cerebellum is organized into three distinct layers: the molecular layer, the Purkinje cell layer, and the granular layer. Each layer has a unique cellular composition and functional role. Changes to these layers, particularly those affecting Purkinje neurons and granular cells, can impact motor coordination and cognitive function [18,19].

Interestingly, AD and T2DM share several characteristics. In fact, some researchers have coined the term "type 3 diabetes" to describe AD as a form of cerebral diabetes [4–6,20,21]. Metformin, a biguanide commonly prescribed as the primary treatment for T2DM, has been shown to have pleiotropic effects beyond its hypoglycemic action. It activates AMP-activated protein kinase (AMPK), which modulates energy metabolism and reduces hepatic glucose production [22,23]. Recently, considerable attention has been given to the potential neuroprotective effects of metformin. Importantly, metformin can cross the BBB, making its potential effects on the central nervous system particularly relevant to the study of diabetes-associated cognitive impairment. Preclinical studies suggest that metformin may improve cognitive function in animal models of T2DM, reduce oxidative stress, and attenuate tau pathology [24–26]. However, evidence regarding its impact on amyloid plaque accumulation is scarce and contradictory [27–29].

Furthermore, sex differences may influence the pathophysiology and clinical manifestations of T2DM and its complications. Epidemiological and clinical studies suggest that women with T2DM are at a higher risk of cognitive impairment and dementia than men with the disease [30,31]. Several factors have been proposed as contributors to this difference. These factors include sex hormones, the apolipoprotein E4 allele (a genetic factor), pregnancy-related complications, and disturbances in mood, sleep, and stress responses [32,33]. However, the mechanisms underlying this increased vulnerability are not fully understood. Thus, the present study focused on characterizing the metabolic, behavioral, and neuropathological effects of metformin in a female mouse model of T2DM. It is important to note that this study was not designed to determine sex-specific responses to metformin or to make direct comparisons with male diabetic mice.

Accordingly, the study examined the effects of metformin on recognition memory and region-specific neuropathological changes in the CA1 region of the hippocampus, the cerebral cortex, and the cerebellum. Additionally, we assessed whether metformin modulates

key biomarkers associated with diabetes-related cognitive impairment. These biomarkers include amyloid and tau proteins, as well as cholesterol and insulin levels in serum and brain tissue. These analyses aimed to provide a more comprehensive characterization of the metabolic, behavioral, and neuropathological effects of metformin in female diabetic mice.

2. Materials and Methods

2.1. Chemical Reagents and Materials

Table 1 lists the chemicals and materials that were used in this study. Metformin was dissolved in a physiological saline solution, and the listed doses refer to its free base form. Streptozotocin (STZ) was dissolved in a citrate buffer solution. All compounds were prepared on the day of use.

Table 1. Reagents and materials used.

Reagents/Materials	Catalog Number	Supplier
Metformin hydrochloride Streptozotocin Nicotinamide	13118 13104 11127	Cayman Chemical, Ann Arbor, MI, USA
Citric acid Sodium citrate dihydrate	251275 SX0445	Sigma Chemical Co., St. Louis, MO, USA
Phosphorylated (S199) tau Total tau protein Amyloid $A\beta_{42}$ Total cholesterol	KMB7041 KMB7011 KMB3441 EEA026	Fisher Scientific, Waltham, MA, USA
Insulin	MBS2708295	MyBioSource, San Diego, CA, USA.
Hematoxylin and eosin stain	64298	Hycel, Zapopan, JAL, Mexico.
Saline solution (0.9%) Isoflurane	Q-7833-009 Q-7833-222	PISA Pharmaceuticals, Guadalajara, JAL, Mexico
Congo red stain	2321-5	Fragalab, Guamuchil, SIN, Mexico
Accu-Chek glucometer Glucose test strips	1996E2017 0679R2017	Roche, Miguel Hidalgo, CDMX, Mexico

2.2. Animals

Eight-week-old BALB/c mice, with an average weight of 22.66 ± 0.47 g, were purchased from the Morelos vivarium (Cuernavaca, MOR, MX). The mice were allowed to acclimate for one week before the start of the study. During this time, they were housed in groups of ten in cages measuring 37 × 47 × 20 cm under a reversed light/dark cycle, which is described below. Their food and water intake was monitored to confirm normal feeding and drinking habits. The animals were regularly handled to habituate them to human contact. This period also allowed for the identification and exclusion of animals showing signs of illness. Subsequently, the healthy mice were randomly housed in groups of three in acrylic rodent cages measuring 19 × 29 × 12 cm. These cages contained wood shavings but no additional enrichment. The light/dark cycle was reversed at 20:00 h, and the temperature was maintained at 23 ± 2 °C with 50–70% relative humidity. The mice had ad libitum access to tap water and SAFE® A30 food (SAFE, Augy, Yonne, France). To induce type 2 diabetes with STZ plus nicotinamide and measure blood glucose levels, the animals were fasted for four hours beforehand. The mice were also fasted overnight before euthanasia to prevent interference with the biochemical measurements. However, they always had

access to water. For behavioral studies, the animals were not fasted. To minimize fear and discomfort, all handling procedures were performed by trained personnel. Injections and sampling were carried out gently and consistently to prevent tissue damage and pain. All research protocols were approved by the Ethics Committee of our institution, and the study adhered to the ARRIVE guidelines for the care and use of animals in research.

A total of 72 animals were randomly divided into six experimental groups. Group 1 consisted of non-diabetic female mice that received citrate buffer and a 0.9% saline solution via intraperitoneal injections (i.p.) (n = 12). Group 2 received STZ and nicotinamide via i.p. injections (the diabetic control group; n = 12). Group 3 consisted of diabetic mice that were treated with a 0.9% saline solution. Groups 4, 5, and 6 consisted of diabetic mice treated with metformin at doses of 50, 150, and 250 mg/kg, respectively. Groups 3, 4, 5, and 6 received their respective treatments daily by oral gavage for 28 days (Figure 1). Each treatment was administered at a volume of 100 µL.

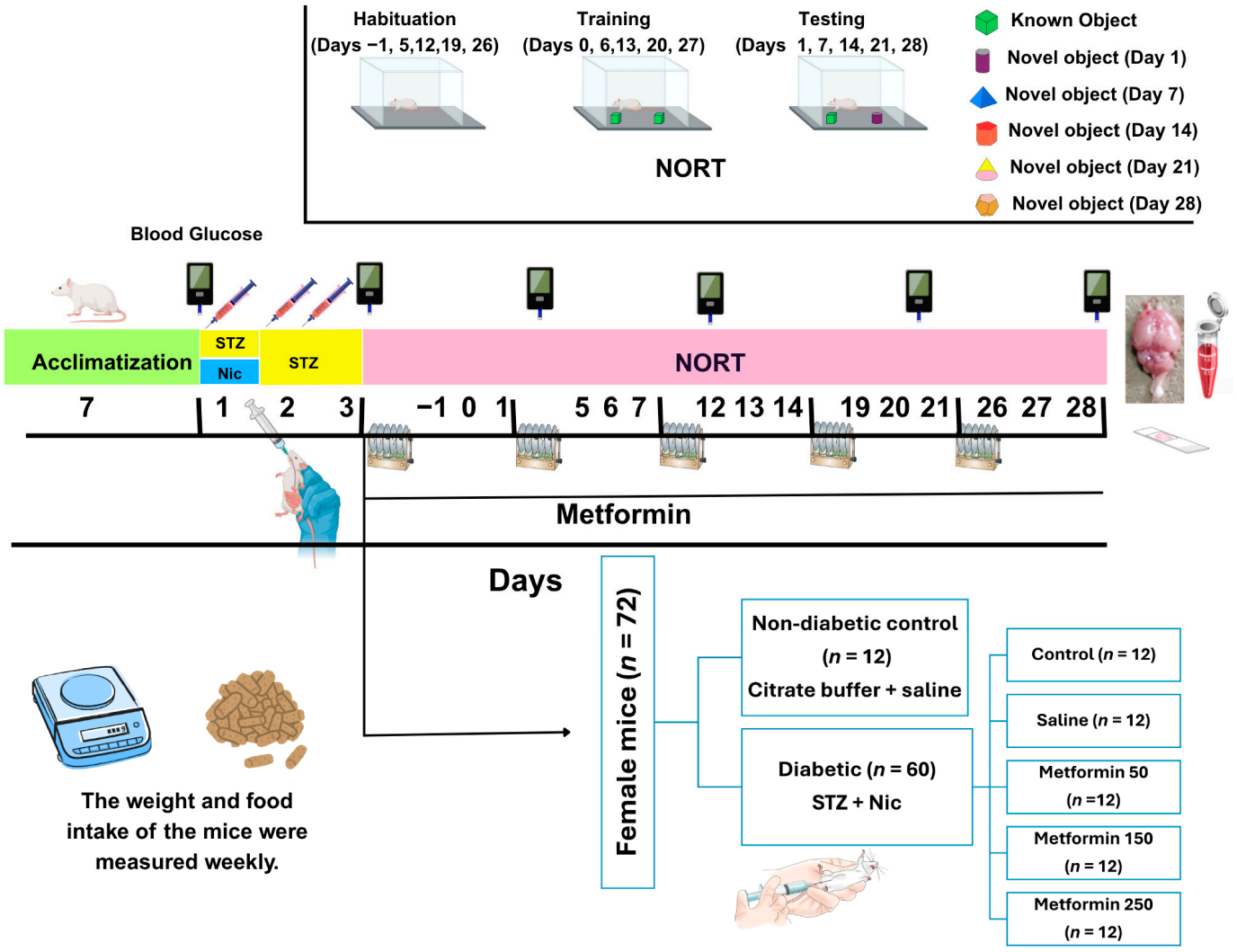


Figure 1. Schematic representation of the experimental protocol. STZ: streptozotocin; Nic: nicotinamide; NORT: Novel object recognition test. Metformin was administered orally (mg/kg).

2.3. Rationale for the Metformin Dosing Used in the Present Study

The metformin doses used in this study were based on the therapeutic range for treating diabetes, which is 500 to 3000 mg/60 kg [34]. We selected one dose below this range (243 mg/60 kg) and two within the range (730 and 1216 mg/60 kg). First, we converted each dose to milligrams per kilogram. Thus, the doses corresponded to 4.05,

12.17, and 20.27 mg/kg, respectively. Next, we calculated the animal equivalent dose (AED) based on body surface area using the following formula [35] (Equation (1)):

$$\text{Animal Equivalent Dose} = \left(\text{Human dose}\frac{\text{mg}}{\text{kg}}\right) \times \left(\frac{\text{Human Km}}{\text{Mouse Km}}\right) \quad (1)$$

K_m is the correction factor, where the human K_m value is 37, and the mouse K_m value is 3.

According to this conversion, the doses of 243, 730, and 1216 mg/60 kg are equivalent to 50, 150, and 250 mg/kg, respectively, in mice. Previous studies have demonstrated that acute (150 mg/kg) or subchronic (300 mg/kg for three weeks) oral administration of metformin reaches various regions of the brain, including the hippocampus, cerebellum, and cortex [36].

2.4. Diabetes Induction

On day 1, 60 mice received an intraperitoneal (i.p.) injection of STZ at a dose of 100 mg/kg. Fifteen minutes later, the mice received a 30 mg/kg dose of nicotinamide via i.p. injection. On days 2 and 3, the mice received an 80 mg/kg dose of STZ daily (Figure 1). In total, the mice received 260 mg/kg of STZ. The STZ was dissolved in a citrate buffer solution containing sodium citrate dihydrate and citric acid at a concentration of 0.1 M and a pH of 4.5. The nicotinamide was dissolved in a 0.9% saline solution. The mice were considered diabetic if their fasting glucose level was 200 mg/dL or higher by day 4, as measured with a glucometer (considered day 1 in the experimental protocol). Glucose levels, food intake, and weight gain were measured at the beginning of the experiment and again on days 1, 7, 14, 21, and 28.

2.5. Novel Object Recognition Test (NORT)

As previously reported [37], the motor function of all the diabetic animals was assessed using the rotarod test prior to the behavioral evaluation. Only those with a comparable latency to fall to that of the non-diabetic control group were included in the study. This ensured that any differences observed in the NORT would reflect cognitive effects rather than motor impairments.

The NORT was performed in a transparent plastic box measuring 40 × 40 × 40 cm over the course of three consecutive days and repeated weekly [37]. The test consisted of three phases: habituation (days −1, 5, 12, 19, and 26; five minutes), training (days 0, 6, 13, 20, and 27; ten minutes), and testing (days 1, 7, 14, 21, and 28; ten minutes) (Figure 1). All trials took place in a dark procedure room lit by a red light. On the first day, each mouse was acclimated to the arena without any objects present. The next day, two identical objects were placed in the arena during the training phase. During the testing phase, one of the objects was replaced with a novel object that differed in material, shape, and color. Each week, the novel object was replaced with a new one of a similar size, but with a different shape and color (Figure 1). The box and objects were cleaned with 70% ethanol and dried between each mouse to avoid olfactory cues. The exploratory behavior of each mouse was recorded using an infrared video camera. Object exploration was defined as sniffing or touching an object with the nose or paws, or pointing the nose at an object from less than one centimeter away. Sitting on or around objects was not considered exploratory behavior. The study only included animals that explored objects for at least 15 s. A researcher who was unaware of the treatments analyzed the recordings and manually recorded how long each mouse spent exploring the objects at each stage. Then, discrimination (Equation (2)) and preference (Equation (3)) indices were calculated using the following equations based on the recorded exploration times [38]:

$$\text{Discrimination index} = \frac{T2 - T1}{T2 + T1} \quad (2)$$

$$\text{Preference index} = \frac{T2}{T2 + T1} \times 100 \quad (3)$$

where T1 is the time spent exploring the known object, and T2 is the time spent exploring the new object. Both times are measured in seconds.

2.6. Quantification of Biochemical Markers

On day 28, after the behavioral evaluations were complete, the mice were euthanized while under deep anesthesia with 4% isoflurane. The adequacy of the anesthesia was confirmed by the absence of pedal and corneal reflexes before intracardiac exsanguination. This method ensured a humane and irreversible death in accordance with ethical standards. Blood samples (n = 12 per experimental group) were collected in 1.5 mL Eppendorf tubes for serum separation. Next, an incision was made in the thoracic cavity, and a catheter was inserted into the left ventricle. Then, the right atrium was incised, and the mice were perfused with phosphate-buffered saline (PBS) until all the remaining blood was completely removed. The brains (n = 12; 0.44 ± 0.02 g) and pancreases (n = 12; 0.14 ± 0.03 g) of each mouse were dissected, frozen at −80 °C, and stored until use. The brains of each experimental group were divided to perform analyses of cholesterol, insulin, and tau protein (n = 4), and insoluble amyloid peptide $A\beta_{42}$ (n = 4). For the biochemical analysis, the brain was cut into smaller pieces using a manual homogenizer. The pieces were then transferred to 50 mL conical tubes containing a lysis buffer solution (PBS, 50 mM Tris-HCl at pH 7.4, 150 mM NaCl, 1% Triton X-100, and a protease inhibitor cocktail) at a mass-to-volume ratio of 1:10. The tubes were shaken on ice at 300 rpm for 30 min. The resulting mixture was then centrifuged at 15,000 *g* for 20 min at 4 °C [37].

2.6.1. Cholesterol Quantification

Serum cholesterol levels were measured using a microplate assay. First, 2.5 µL of the sample was added, followed by 250 µL of the enzyme working solution. After incubating the sample for 10 min at 37 °C, the absorbance was measured at 510 nm.

2.6.2. Insulin Quantification

Prior to the assay, the serum and brain homogenate samples were diluted tenfold in 0.01 M PBS (pH 7.0–7.2). Then, 25 µL of each sample was added to each well of the microplate. Immediately afterward, 25 µL of detection reagent A was added. After incubating for one hour at 37 °C and performing three washes, 50 µL of detection reagent B was added. The plate was then incubated for 30 min at 37 °C and underwent five additional washes. Next, 50 µL of TMB substrate solution was added, and the plate was incubated in the dark at 37 °C for 10–20 min. The reaction was stopped with 25 µL of stop solution, and the absorbance was read at 450 nm.

2.6.3. Quantification of Total and Phosphorylated Tau Protein

The brain homogenate samples were diluted 1:6400 for total tau and 1:200 for phosphorylated tau at site S199 (pS199) in a standard buffer solution. The assay was performed by adding 100 µL of each sample to the wells of an antibody-coated plate. After incubating the plate on an orbital shaker at 500 rpm for two hours at room temperature, the plate was washed four times with 1x wash buffer. Then, 100 µL of biotin conjugate was added and incubated for one hour. Next, 100 µL of streptavidin-HRP was added, and the plate was incubated for 30 min. Finally, 100 µL of TMB substrate solution was added, and the plate was incubated in the dark for 30 min. Four washes were performed between each addition.

The reaction was stopped with 100 µL of stop solution, and the absorbance was measured at 450 nm.

2.6.4. Quantification of Insoluble Amyloid Peptide $A\beta_{42}$

The insoluble fraction of the $A\beta_{42}$ peptide was obtained using a sequential extraction protocol. Briefly, 0.1 g of brain tissue was homogenized in nine volumes of cold PBS (0.01 M, pH 7.4), supplemented with 1 mM AEBSF, a serine protease inhibitor. The mixture was then centrifuged at 14,000 *g* for 45 min at 4 °C. The resulting supernatant (the soluble fraction) was discarded, and the pellet was retained for extraction of the insoluble fraction. The pellet was resuspended in eight volumes of cold 5 M guanidine HCl/50 mM Tris-HCl (pH 8.0), added in 50–100 µL aliquots with homogenization performed after each addition. The mixture was rotated at room temperature for four hours. Then, the mixture was centrifuged at 16,000 *g* for 20 min at 4 °C. The resulting supernatant constituted the insoluble $A\beta_{42}$ fraction. Prior to the ELISA analysis, the $A\beta_{42}$ fraction was diluted 1:10 with the kit's standard diluent buffer to reduce the guanidine concentration to levels compatible with the assay ($\leq$0.5 M). Additionally, AEBSF was added to all dilutions at a final concentration of 1 mM to prevent proteolytic degradation of the peptide. Then, 100 µL of the samples were added to the antibody-coated wells and incubated for two hours at room temperature. This was followed by four washes with 1x wash buffer. Subsequently, 100 µL of the $A\beta_{42}$ detection antibody was added, and the plate was incubated for one hour. After four additional washes, 100 µL of the antibody detection reagent was added, and the plate was incubated for 30 min. The plate was then washed four more times. Finally, 100 µL of TMB solution was added, and the plate was incubated in the dark for 30 min. The reaction was stopped by adding 100 µL of stop solution. Absorbance was read at 450 nm.

2.7. Histological Analyses of the Pancreas and Brain of Diabetic Female Mice

Twelve samples were used for the pancreas and four for the brain. The tissues were fixed in a solution of 4% paraformaldehyde in 0.1 M PBS (pH 7.4) for 24 or 72 h at 4 °C, respectively. Transverse sections of the splenic region of the pancreas were manually obtained. The brains were bisected with a stainless-steel rodent brain matrix (Stoelting Co., Wood Dale, IL, USA) at 1 mm intervals to obtain parasagittal sections. The samples were then dehydrated in ethanol gradients (70%, 80%, 96%, and 100%) and embedded in paraffin. Next, we used a rotary microtome to obtain 5- and 10 µm thick slides of the pancreas and brain, respectively. We mounted these sections on positively charged slides. The slides were deparaffinized in xylene and rehydrated in a series of ethanol solutions of decreasing concentration (100%, 96%, and 80%), followed by distilled water. The slides were stained with Harris's hematoxylin for eight minutes. Then, they were rinsed in running water and differentiated in acid alcohol. After further washing in water, we counterstained the slides with a 0.5% aqueous solution of eosin Y for three minutes. Finally, we dehydrated the slides using successive ethanol baths (96% and 100%), rinsed them in xylene, and mounted them with synthetic resin.

Five randomly selected fields from the total surface area of each pancreas slide were analyzed. Anatomical landmarks were used to identify brain regions in all animals. First, the cerebellum was located, followed by the CA1 region of the hippocampus. Then, a neocortical field, located immediately adjacent to the hippocampus, was taken from the cerebral cortex. This field included the pial surface and cortical layers I-VI. Five fields per sample were analyzed within these regions. A blind analyst performed field selection and scoring. The following variables were considered: edema, inflammation, vacuolization, and necrosis. Depending on the extent of the damage, scores for these variables ranged from 0 to 4 for pancreatic tissue [39,40] and the molecular, Purkinje, and granular layers

of the cerebellum [41,42], and from 1 to 4 for the cerebral cortex [43]. Overall scores corresponding to these parameters were obtained. Neuronal damage in the CA1 region of the hippocampus was assessed based on the degree of damage. Grade 0 indicates an absence of damage, grade 1 scattered damaged neurons, grade 2 a moderate number of damaged neurons (less than 50% affected), and grade 3 severe damage to CA1 pyramidal cells (more than 50% affected) [44].

To perform Congo red staining, which identifies amyloid deposits, the 10 µm thick slides were deparaffinized and rehydrated. Then, they were incubated in a solution of 0.5% Congo red in 50% alcohol for 20 min. The sections were rapidly differentiated in an alkaline alcohol solution (50% ethanol and 0.1% sodium hydroxide) for one minute. After washing with water, the sections were counterstained with Harris's hematoxylin for 30 s. Finally, the sections were dehydrated and cleared with xylene before mounting. All preparations were analyzed and photographed under an optical microscope. The intensity of Congo red staining was quantified using ImageJ software 1.54g (National Institutes of Health, Bethesda, MD, USA).

2.8. Statistical Analysis

All data are expressed as the mean ± standard error. The Shapiro–Wilk test revealed that all behavioral and biochemical datasets followed a normal distribution. To analyze the effects of metformin on blood glucose, weight, food intake, and memory over time, we performed a repeated-measures ANOVA, followed by pairwise comparisons with a Bonferroni correction. To analyze biochemical markers and amyloid-like deposits in the brains of female mice, we performed a one-way ANOVA followed by a Tukey post hoc test. We analyzed histological scores from the pancreas, the CA1 region of the hippocampus, the cerebral cortex, and the cerebellum using the nonparametric Kruskal–Wallis test followed by Dunn's multiple comparisons test. A p-value of less than 0.05 was considered statistically significant in all cases. All statistical analyses were performed using GraphPad Prism version 8.0 (GraphPad Software, San Diego, CA, USA).

3. Results

3.1. Effect of Metformin on Glucose, Body Weight, and Food Intake in Female Type 2 Diabetic Mice

Non-diabetic animals that received citrate buffer plus saline maintained stable glucose levels (77 ± 11 mg/dL) throughout the study. In contrast, animals that received STZ plus nicotinamide had high glucose levels on day 1 (210 ± 32 mg/dL), which gradually increased to 533 ± 21 mg/dL by day 21. By day 28, blood glucose levels decreased slightly to 432 ± 14 mg/dL (Figure 2A). Notably, the STZ + nicotinamide regimen resulted in an 87% survival rate up to day 28.

As expected, orally administering saline solution to diabetic animals did not lower their blood glucose levels. In contrast, administering metformin at doses of 50–250 mg/kg significantly reduced blood glucose levels at the evaluated time points. However, after 14 days, the 50- and 150 mg/kg doses produced a more pronounced hypoglycemic effect (Figure 2A).

The weight of the non-diabetic mice remained stable throughout the evaluation period. The diabetic mice lost significant weight between days 7 and 21. However, by day 28, the diabetic mice had gained weight significantly compared to the non-diabetic female mice. The same response profile was observed in diabetic mice treated with saline. Diabetic mice treated with metformin lost significant weight compared to non-diabetic mice on days 7, 14, and 21, similar to the response observed in the diabetic mice. However, by day 28, their weight was not statistically different from that of the non-diabetic mice, though it was significantly lower than that of the diabetic mice (Figure 2B).

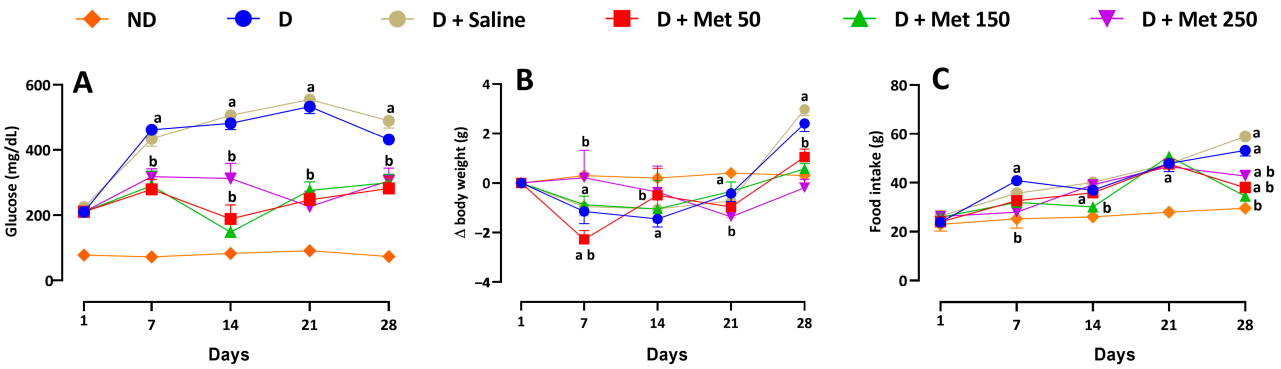


Figure 2. Evaluation of the effect of metformin administration (50, 150, and 250 mg/kg) for 28 days on levels of (**A**) blood glucose, (**B**) body weight, and (**C**) food intake in female diabetic mice. ND: Non-diabetic mice (n = 12); D: Diabetic mice (n = 12); Saline solution (0.9%) (n = 12); Met: Metformin (mg/kg) (n = 12). a: $p < 0.05$ vs. non-diabetic female mice; b: $p < 0.05$ vs. diabetic female mice.

The food consumption of the non-diabetic female mice remained consistent throughout the evaluation period. However, the diabetic mice and the mice treated with saline consumed significantly more food. Mice treated with metformin increased their food consumption until day 21. By day 28, however, food consumption decreased significantly in diabetic mice treated with all doses of metformin compared to untreated diabetic mice. Notably, the food consumption of the mice treated with 150 mg/kg of metformin was similar to that of non-diabetic mice (Figure 2C).

3.2. Effect of Metformin on Recognition Memory of Female Type 2 Diabetic Mice

No significant differences in discrimination or preference indices were observed among the groups on day 1 (Figure 3A,B). However, all groups exhibited negative discrimination index values. From day 7 onward, the diabetic and saline-treated diabetic groups continued to show negative discrimination index values and preference indices below 50%. This indicates a sustained deterioration in recognition memory performance due to diabetes. Although a negative discrimination index alone does not indicate a recognition memory deficit, the persistence of negative discrimination index values and preference index values below 50% in the diabetic groups was consistent with impaired recognition memory performance. Metformin treatment progressively improved both the discrimination and preference indices over time. On day 7, only the 250 mg/kg dose produced a positive discrimination index (Figure 3A). Starting on day 14, all metformin doses significantly increased the discrimination index compared to the diabetic group. By day 28, all three metformin doses produced similar discrimination index values of approximately 0.5 (Figure 3A), while the preference index reached approximately 70% (Figure 3B). Thus, the improvement in recognition memory performance appears to be more closely related to treatment duration than to metformin dosage.

3.3. Effect of Metformin on the Cholesterol, Tau Protein and Insulin Levels in Female Type 2 Diabetic Mice

Serum cholesterol levels increased 20- to 22-fold in both untreated and saline-treated female diabetic mice compared to non-diabetic mice (an increase from 80 mg/dL to 1610–1767 mg/dL). A low dose of metformin (50 mg/kg) did not reverse the increase in serum cholesterol levels in diabetic mice. However, metformin doses of 150 and 250 mg/kg significantly reduced serum cholesterol levels to 320–330 mg/dL (Figure 4A).

Serum insulin concentrations were significantly higher in diabetic female mice than in non-diabetic female mice (Figure 4B). In contrast, the insulin concentration in the brains of diabetic female mice was significantly lower (Figure 4C). Administering metformin at any

dose reversed the increase in serum insulin and prevented the decrease in brain insulin in diabetic female mice.

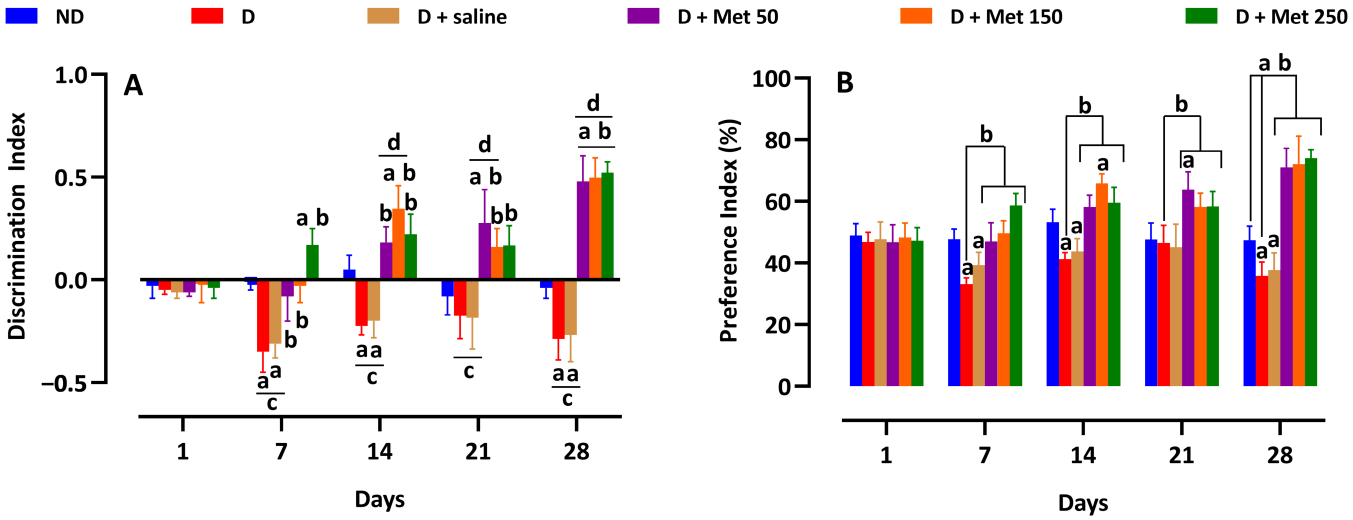


Figure 3. Evaluation of recognition memory in female mice using the Novel Object Recognition Test (NORT). (**A**) Discrimination and (**B**) preference indices were calculated to compare recognition memory performance. ND: Non-diabetic female mice (n = 12); D: Diabetic female mice (n = 12); Saline solution (0.9%) (n = 12); Met: Metformin (mg/kg) (n = 12). a: $p < 0.05$ vs. non-diabetic female mice; b: $p < 0.05$ vs. diabetic female mice; c: $p < 0.05$ vs. basal discrimination index (day 1); d: $p < 0.05$ vs. discrimination index on day 7.

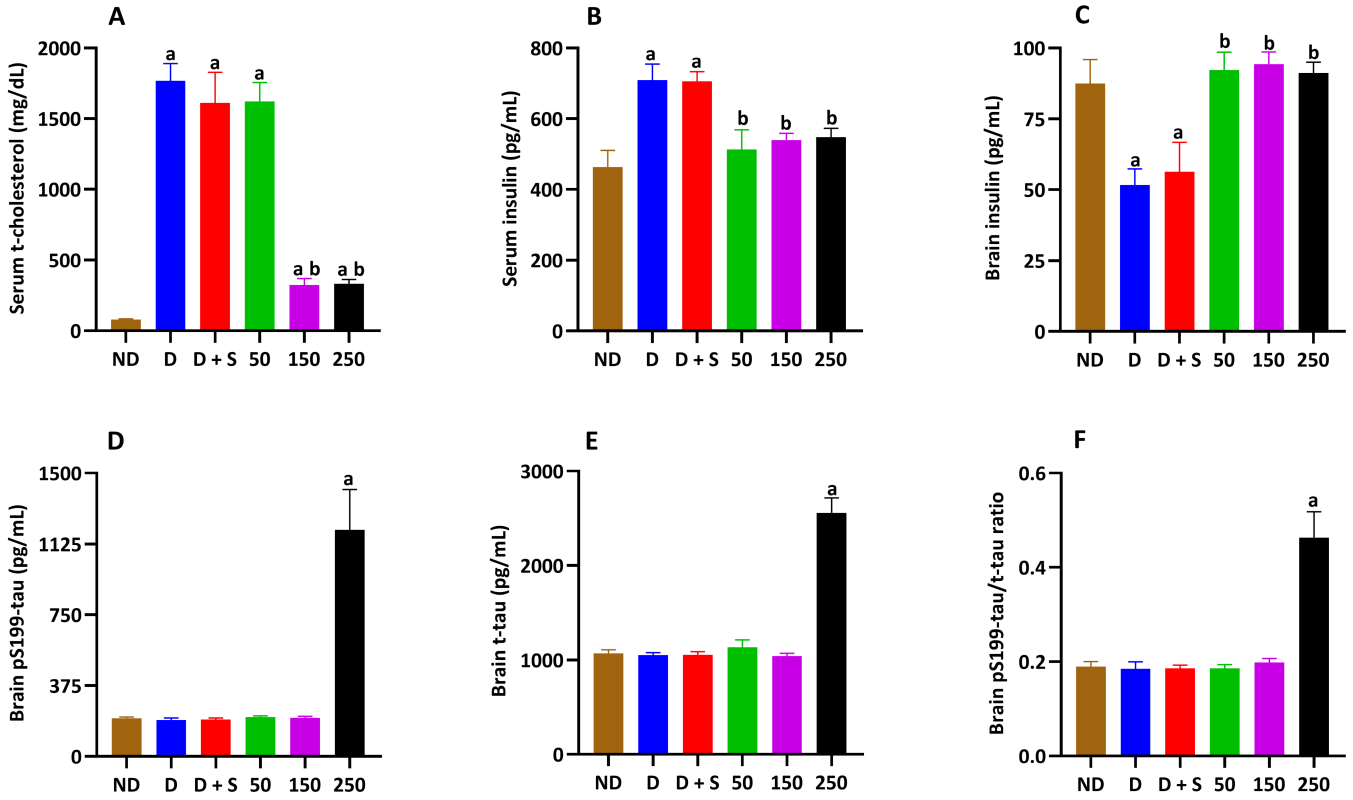


Figure 4. Evaluation of the effect of metformin administration (50, 150, and 250 mg/kg) for 28 days on levels of (**A**) cholesterol in serum (n = 12), (**B**,**C**) insulin in serum (n = 12) and brain (n = 4), and (**D**) phosphorylated tau (pS199) (n = 4) and (**E**) total tau protein (n = 4) and its ratio (**F**) in brain homogenates of diabetic mice (n = 4). ND: Non-diabetic mice; D: Diabetic mice; S: Saline solution (0.9%); a: $p < 0.05$ vs. non-diabetic female mice; b: $p < 0.05$ vs. diabetic female mice.

Treatment with up to 150 mg/kg of metformin did not affect tau protein levels (Figure 4D,E). However, treatment with 250 mg/kg significantly increased the levels of both phosphorylated and total tau proteins in the brains of female diabetic mice (Figure 4D,E). The ratio of phosphorylated tau protein to total tau protein exhibited a similar pattern (Figure 4F). These results suggest that the highest dose of metformin may have unfavorable effects on tau-related markers.

3.4. Effect of Metformin on the Morphology of the Pancreas, CA1 Region of the Hippocampus, and the Cerebral Cortex and Cerebellum of Female Type 2 Diabetic Mice

In non-diabetic mice, the islets of Langerhans exhibited distinct borders and an appropriate cellular density. The pancreatic acini exhibited organized architecture with a uniform arrangement and a characteristic eosinophilic cytoplasm (Figure 5A). In contrast, the islets in the untreated diabetic group showed marked morphological alterations, including loss of definition, reduced size, and decreased cellularity. In some areas, the islets were difficult to distinguish from the surrounding tissue (Figure 5B). The acini showed structural disorganization and acquired a more diffuse appearance, losing their typical pattern. The presence of an inflammatory infiltrate was evidenced by small, scattered basophilic cells, which are consistent with lymphocytic infiltration. A pattern similar to that of the untreated diabetic group was observed in the diabetic group treated with saline solution (Figure 5C).

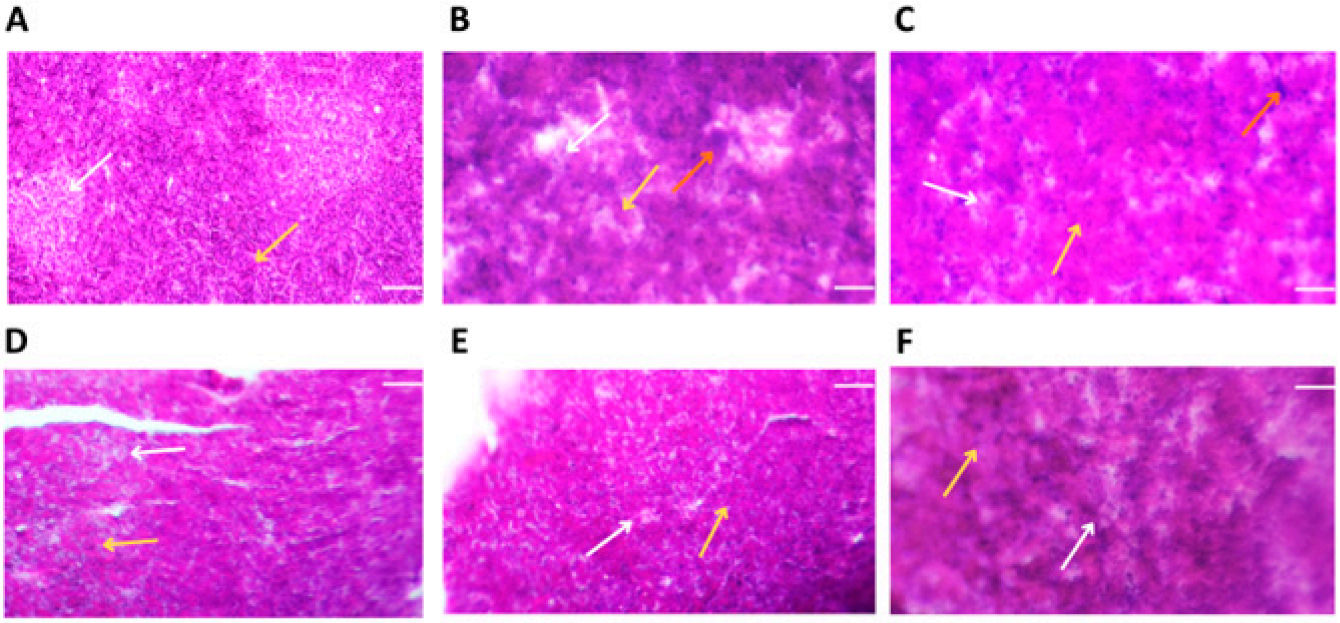


Figure 5. Representative micrographs (40×) of hematoxylin and eosin staining in the pancreas of female mice. (**A**) Non-diabetic mice (n = 12), (**B**) diabetic mice (n = 12), (**C**) diabetic mice treated with saline solution (0.9%) (n = 12), and diabetic mice treated with metformin (**D**) 50 (n = 12), (**E**) 150 (n = 12), and (**F**) 250 mg/kg (n = 12), respectively. The white arrow indicates the islets of Langerhans, the yellow arrow indicates the pancreatic acini, and the orange arrow indicates lymphocyte infiltration. The white scale bar represents 10 μm.

Metformin administration failed to fully restore the morphology of the islets of Langerhans (Figure 5D–F). These islets were smaller and had lower cellular density than those of the non-diabetic control group. There was a slight improvement in exocrine tissue organization, but the pancreatic acini did not achieve a morphology comparable to that of a non-diabetic pancreas (Figure 5A). One of the most evident effects of the treatment was the reduction in lymphocytic infiltration. This reduction may indicate a decrease in the inflammatory response associated with pancreatic damage, despite the absence of structural

recovery of the islets in diabetic mice. Accordingly, the cytostructural score of this tissue showed that metformin provides a certain degree of protection against pancreatic damage caused by experimental diabetes in a dose-dependent manner. However, metformin did not prevent chemical damage to the pancreas induced by streptozotocin (Figure 6A).

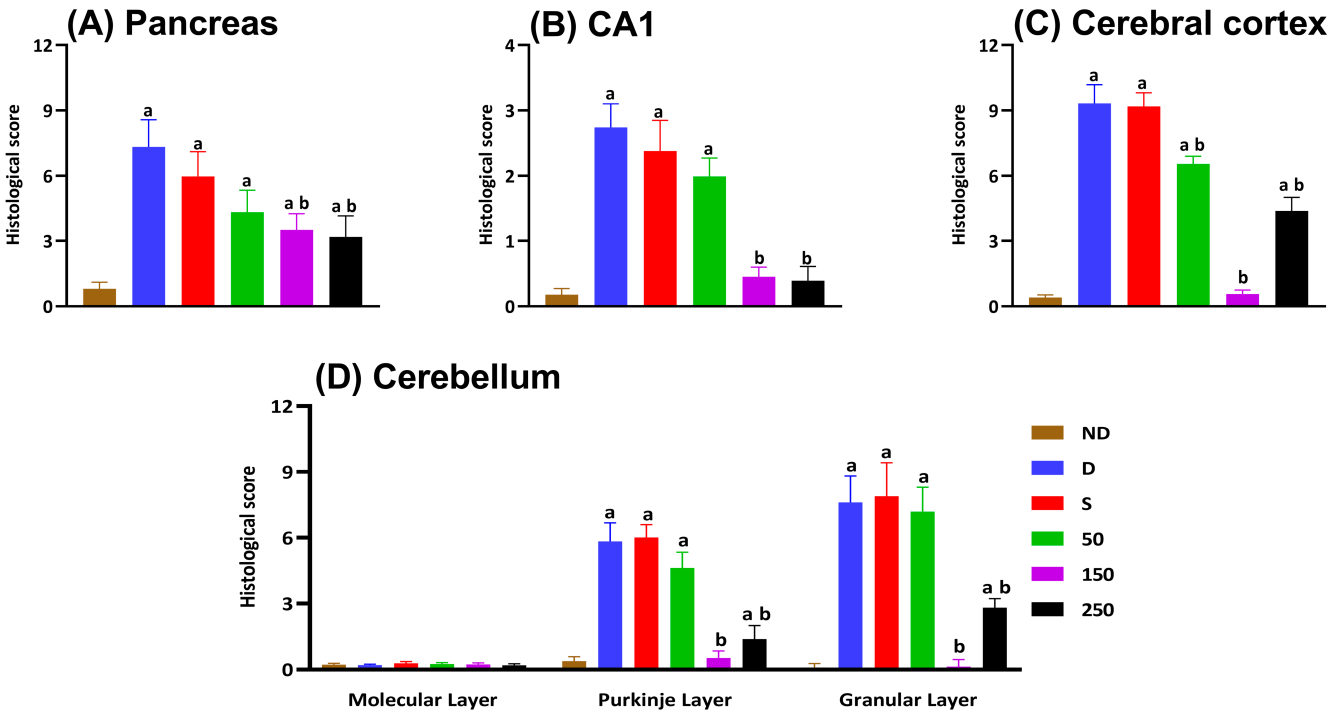


Figure 6. Histological score obtained with micrographs of hematoxylin and eosin staining in the (**A**) pancreas and cerebral regions such as (**B**) CA1, (**C**) cerebral cortex, and (**D**) cerebellum of female mice. ND: Non-diabetic mice; D: Diabetic mice; S: Saline solution (0.9%); Metformin (50, 150, and 250 mg/kg); a: $p < 0.05$ vs. non-diabetic female mice; b: $p < 0.05$ vs. diabetic female mice.

In non-diabetic female mice, the pyramidal layer of the Cornu Ammonis 1 (CA1) region of the hippocampus contained pyramidal neurons with large, rounded, or ovoid cell bodies arranged in an orderly and compact manner (Figure 7A). Diabetes induced degenerative changes in the CA1 pyramidal neurons of female mice (Figure 7B). These changes included decreased cell density, neuronal loss, pyknotic cells with irregular contours, and disorganized pyramidal layers (Figure 7B,C).

In contrast, diabetic animals treated with 50 mg/kg of metformin showed partial recovery of neuronal architecture (Figure 7D). These neurons exhibited less pyknosis than those in the untreated diabetic groups, though residual degenerative signs persisted. Groups treated with 150 or 250 mg/kg of metformin exhibited the greatest histological recovery (Figure 7E,F). These groups had a CA1 region organized similarly to the control group (Figure 7A), with neurons that had preserved morphology and were arranged in an orderly fashion. These neurons showed minimal evidence of pyknosis. Metformin protected the CA1 region of the hippocampus from diabetes-induced damage. This protection occurred at the 150- and 250 mg/kg doses, as indicated by morphological change scores (Figure 6B).

The cortical cells of the non-diabetic female mice showed an eosinophilic cytoplasm and large, round, pale nuclei. The neuropil appeared uniform, with no empty spaces or vacuolization (Figure 8A). In contrast, mild disorganization of the cortical layers, accompanied by a loss of layer definition, was observed in diabetic mice. There was also a reduction in neuronal density. Many neurons exhibited nuclear pyknosis, characterized by small, hyperchromatic, dark purple nuclei, indicating apoptosis or cellular stress (Figure 8B). Additionally, vacuolization and edema were present, indicating tissue damage and in-

flammation. The same morphology was observed in diabetic animals treated with saline (Figure 8C) or metformin at 50 mg/kg (Figure 8D) and 250 mg/kg (Figure 8F). However, the cortical layers were more clearly defined in the cerebral cortex of diabetic mice treated with 150 mg/kg of metformin (Figure 8E). The tissue architecture of this group more closely resembled that of the non-diabetic control group (Figure 8A). This improvement was not evident in the 250 mg/kg group (Figure 8F), which is consistent with the histological scores (Figure 6C).

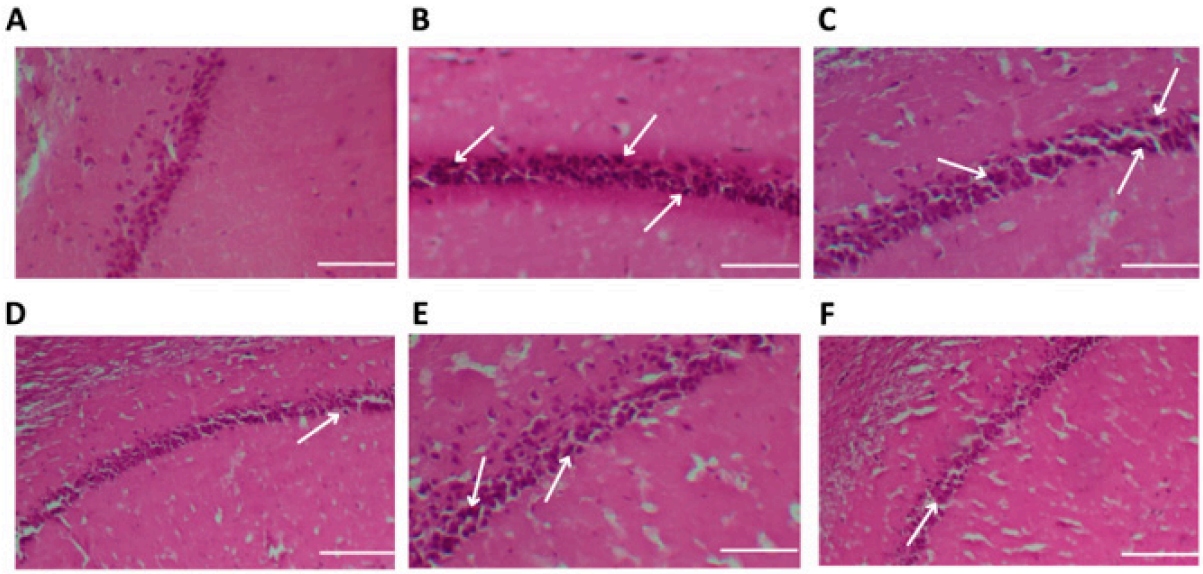


Figure 7. Representative micrographs (40×) of hematoxylin and eosin staining in the Cornu Ammonis 1 (CA1) region of the hippocampus of female mice. (**A**) Non-diabetic mice (n = 4), (**B**) diabetic mice (n = 4), (**C**) diabetic mice treated with saline solution (0.9%) (n = 4), and diabetic mice treated with metformin (**D**) 50 (n = 4), (**E**) 150 (n = 4), and (**F**) 250 mg/kg (n = 4), respectively. The white arrow indicates the presence of pyknosis. The white scale bar represents 50 µm.

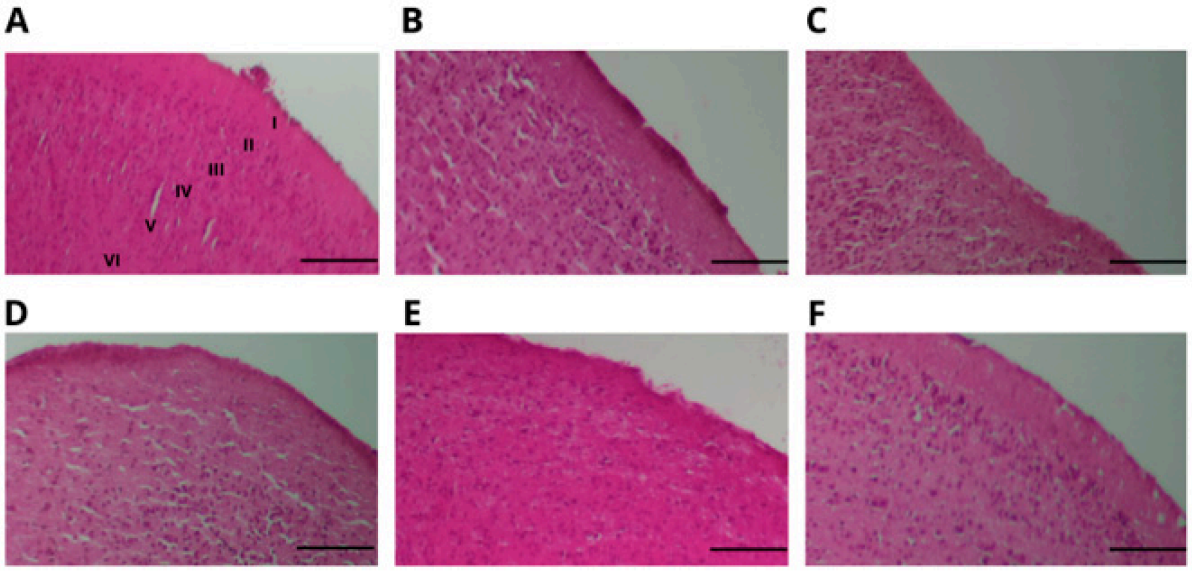


Figure 8. Representative micrographs (4×) of hematoxylin and eosin staining in the cerebral cortex of female mice. (**A**) Non-diabetic mice (n = 4), (**B**) diabetic mice (n = 4), (**C**) diabetic mice treated with saline solution (0.9%) (n = 4), and diabetic mice treated with metformin (**D**) 50 (n = 4), (**E**) 150 (n = 4), and (**F**) 250 mg/kg (n = 4), respectively. The black arrow indicates the presence of pyknosis. The black scale bar represents 200 µm. (I) Molecular layer; (II) Outer granular layer; (III) Outer pyramidal layer; (IV) Inner granular layer; (V) Inner pyramidal layer; (VI) Multiform layer.

The cerebellum of non-diabetic female mice had three clearly distinguishable layers. The external molecular layer had a low cell density. The Purkinje cell layer contained single cells with large cell bodies and abundant cytoplasm. The granular layer had a high density of small, uniformly distributed nuclei. No signs of damage or inflammation were observed in this group (Figure 9A).

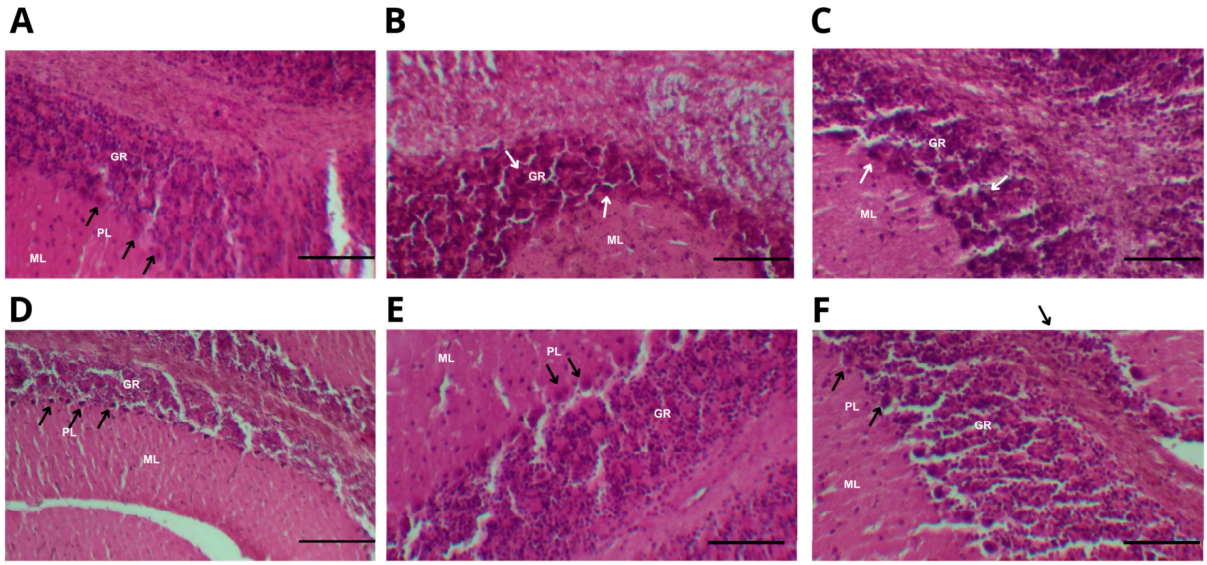


Figure 9. Representative micrographs (40×) of hematoxylin and eosin staining in the cerebellum of female mice (n = 4). (**A**) Non-diabetic mice (n = 4), (**B**) diabetic mice (n = 4), (**C**) diabetic mice treated with saline solution (0.9%) (n = 4), and diabetic mice treated with metformin (**D**) 50 (n = 4), (**E**) 150 (n = 4), and (**F**) 250 mg/kg (n = 4), respectively. The black arrow indicates the Purkinje layer, and the white arrow indicates the presence of pyknosis. The black scale bar represents 30 µm. (ML) Molecular layer; (PL) Purkinje layer; (GR) Granular layer.

Decreased cell density in the granular layer and nuclear pyknosis were observed in diabetic female mice (Figure 9B). Additionally, loss and degeneration of Purkinje cells were evident. Treatment with a saline solution (Figure 9C) did not prevent these morphological alterations. In the brains of animals treated with 50 mg/kg of metformin (Figure 9D), the Purkinje layer was identifiable but still contained pyknotic cells. The granular layer showed slight improvement in density, evidenced by fewer pyknotic cells. However, this improvement was not statistically significant (Figure 6D). With the administration of 150 mg/kg of metformin, nearly complete recovery of the cerebellar architecture was observed (Figure 9E). Animals treated with 250 mg/kg of metformin showed improved granular layer density, suggesting partial prevention of damage in this brain region (Figures 6D and 9F). However, some Purkinje cells showed signs of pyknosis (Figure 9F). Notably, no damage was observed in the molecular layer of the cerebellum of diabetic animals, as demonstrated by the histological score (Figure 6D).

3.5. Effect of Metformin on Amyloid-like Deposits in the CA1 Region of the Hippocampus, Cerebral Cortex, and Cerebellum of Female Type 2 Diabetic Mice

Staining of the CA1 region of the hippocampus and the cerebral cortex of non-diabetic female mice revealed minimal Congo red-positive deposits (Figure 10A,B). Congo red-positive deposits were observed in the cerebellum, specifically in the Purkinje and granular layers (Figure 10). Groups treated with metformin exhibited reduced Congo red staining in a dose-dependent manner. The 250 mg/kg dose completely prevented the appearance of Congo red-positive deposits (Figure 10C).

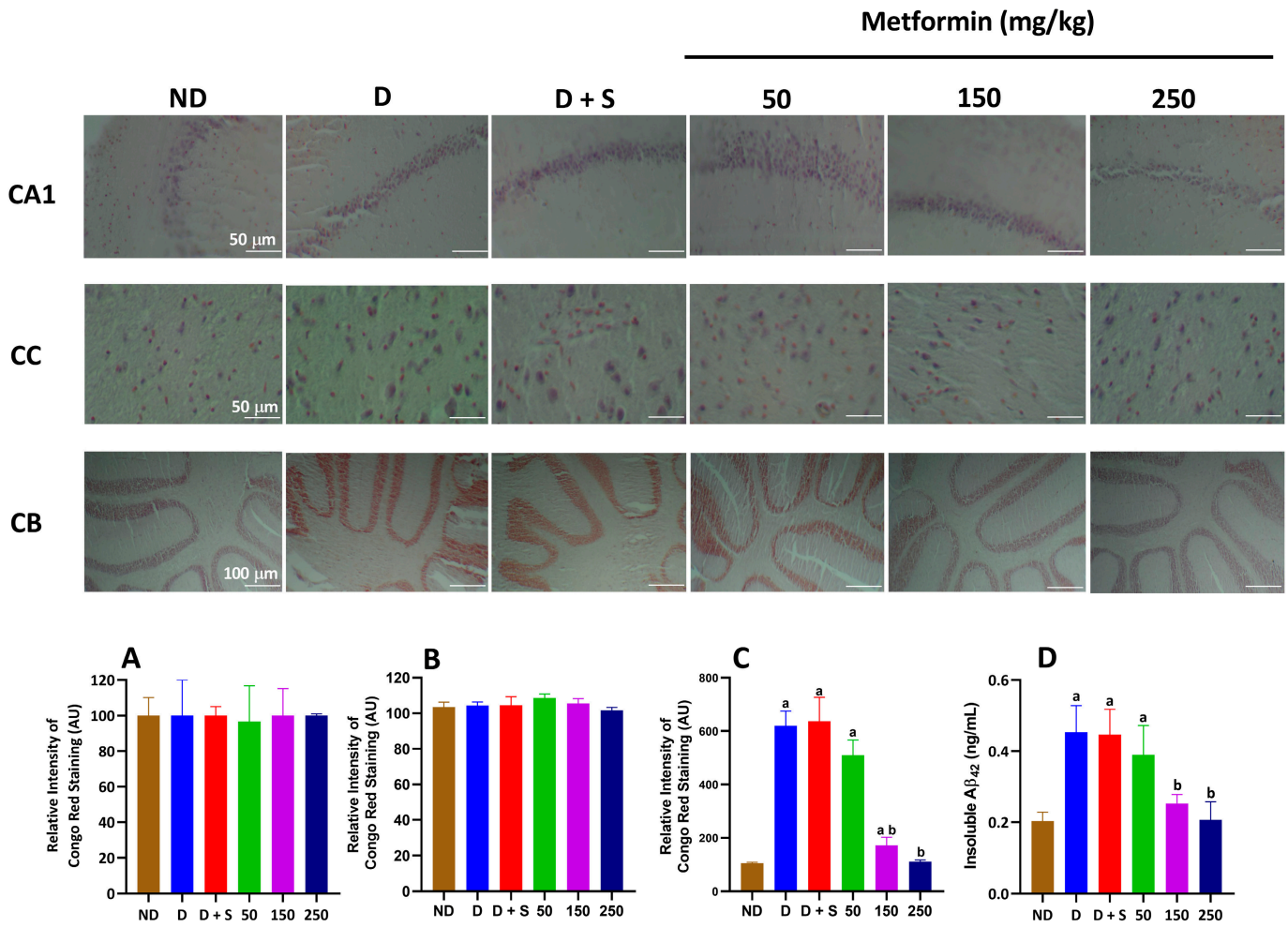


Figure 10. Representative micrographs of Congo red staining in the Cornu Ammonis 1 of the hippocampus (CA1, 40×), cerebral cortex (CC, 40×), and cerebellum (CB, 4×) of female mice, $n = 4$ for each experimental group. The corresponding quantification of Congo red staining is shown in (**A**) CA1, (**B**) cerebral cortex, and (**C**) cerebellum. (**D**) Quantification of insoluble $A\beta_{42}$ fraction in whole brain homogenates. ND: Non-diabetic mice ($n = 4$); D: Diabetic mice ($n = 4$); D + S: Diabetic mice treated with saline ($n = 4$). a: $p < 0.05$ vs. non-diabetic female mice; b: $p < 0.05$ vs. diabetic female mice.

The insoluble $A\beta_{42}$ fraction was significantly higher in the brain homogenates of diabetic mice than in the control group. Treatment with metformin reduced the levels of the insoluble $A\beta_{42}$ fraction in a dose-dependent manner (Figure 10D). This pattern is consistent with the reduction in amyloid burden observed by Congo red staining in the cerebellum (Figure 10C). However, it should be noted that regional quantification of $A\beta_{42}$ levels in specific areas such as the CA1 region, cerebral cortex, and cerebellum was not performed.

4. Discussion

4.1. Effectiveness of the Type 2 Diabetes Mellitus Model and Systemic Effects of Metformin

The diabetes induction protocol used in this study differs from the more commonly cited ratios of 1:1.5 to 1:5 of STZ and nicotinamide in male rodents [45], since these ratios did not produce sustained hyperglycemia in female mice during preliminary testing. BALB/c mice exhibit greater resistance to β-cell toxicity [46–48]. This difference may be due to varying susceptibility to STZ depending on the mouse strain or sex. Our protocol involves a cumulative dose of 260 mg/kg of STZ and a 30 mg/kg dose of nicotinamide, yielding an

STZ/nicotinamide ratio of approximately 8.6:1. Using this protocol, female mice achieved sustained hyperglycemia for 28 days with a 13% mortality rate.

Importantly, the metabolic profile observed in the female diabetic mice is consistent with type 2 diabetes rather than type 1. These mice exhibited hyperglycemia, hyperinsulinemia, and dyslipidemia, indicating preserved pancreatic insulin production and a compensatory response that is consistent with insulin resistance. Additionally, histological examination revealed a reduction in pancreatic islet size, though not complete β-cell destruction. These findings suggest partial β-cell dysfunction as opposed to the absolute insulin deficiency typically observed in type 1 diabetes models. Therefore, despite the relatively high cumulative dose of STZ, the combination with nicotinamide produced a phenotype characterized by severe metabolic dysregulation and residual insulin production. This phenotype is consistent with those previously described in experimental models of advanced type 2 diabetes. Furthermore, the diabetic mice displayed polyphagia and changes in body weight, which are phenotypic characteristics of T2DM [49]. Thus, the STZ-nicotinamide model replicates some of the key metabolic features of type 2 diabetes.

As previously reported, metformin reduces blood glucose levels in female diabetic mice [50]. A 150 mg/kg dose of metformin achieved robust glycemic control without causing hypoglycemia, and it restored food intake to control group levels by the end of the treatment. This is significant because weight management and appetite control are important considerations in T2DM treatment [49,51]. As previously reported in rodents, diabetes induces a dramatic increase in total cholesterol levels (approximately 20-fold) [52]. Although metformin did not fully reverse this increase, the 150- and 250 mg/kg doses significantly reduced it. Considering the role of dyslipidemia in BBB dysfunction and Alzheimer's disease pathogenesis [10], the ability of metformin to attenuate dyslipidemia may contribute to its potential neuroprotective effects. Reducing peripheral cholesterol may help maintain BBB integrity by limiting the entry of circulating factors that may promote neuroinflammation and protein aggregation [53]. These changes, in turn, create a less favorable environment for amyloid accumulation.

Our results support the effectiveness of the T2DM model. Diabetic mice exhibited significant alterations in insulin homeostasis characterized by hyperinsulinemia in the blood and significantly reduced insulin levels in brain tissue [24,54]. These alterations are consistent with the development of systemic insulin resistance and impaired cerebral insulin homeostasis, both of which have been reported in experimental models of T2DM [55]. Together with the hyperglycemia and metabolic alterations observed in the diabetic animals, these findings suggest that the streptozotocin–nicotinamide protocol effectively mimics the metabolic features of T2DM.

Treatment with metformin normalized serum insulin levels and prevented the reduction in brain insulin levels observed in diabetic mice at all doses tested. These results suggest that metformin improves systemic and cerebral insulin homeostasis. However, it is important to note that metformin did not restore normal pancreatic architecture at any of the tested doses. Thus, the improvement in insulin homeostasis occurred despite persistent structural alterations in the pancreas and was not accompanied by recovery of pancreatic architecture. These effects may reflect metformin's established metabolic actions, including the suppression of hepatic gluconeogenesis and the improvement of insulin sensitivity in peripheral tissues [56]. Overall, these findings suggest that metformin may attenuate metabolic disturbances associated with diabetes without restoring the underlying pancreatic structural abnormalities.

4.2. The Neuroprotective Effects of Metformin in the Brains of Female Mice

T2DM has been associated with neuronal damage in the hippocampus, cerebral cortex, and cerebellum [57]. In the present study, metformin reduced the extent of neuronal damage observed in these brain regions. This finding is consistent with previous studies in male rats and female mice with AD [58,59]. Of the tested doses, 150 mg/kg showed a significant protective effect on structural integrity. Previous studies have also reported increased Aβ accumulation in non-transgenic diabetic rodents [60–62]. However, murine Aβ differs from human Aβ by three amino acid residues and has a lower propensity to aggregate [63]. Therefore, increased insoluble $A\beta_{42}$ in brain homogenates alone does not prove Aβ aggregation or plaque formation [64,65]. Conversely, Congo red staining provides evidence of cerebellar amyloid deposition, but it does not prove that the deposits are exclusively composed of $A\beta_{42}$ [66]. Accordingly, these findings are best interpreted as evidence of amyloid-like pathology rather than as definitive evidence of $A\beta_{42}$ plaque formation. Metformin may reduce this amyloid-like pathology by mechanisms that create a less favorable environment for protein aggregation and associated neurotoxicity. In this regard, it has been reported that metformin reduces the accumulation of Aβ in the cortex and hippocampus of male transgenic AD mice through mechanisms involving AMPK and insulin-degrading enzyme (IDE) signaling [67]. Whether these mechanisms operate in the cerebellum of diabetic female mice requires further investigation.

Interestingly, higher doses of metformin (150 and 250 mg/kg) reduced amyloid-like deposits in the Purkinje and granular layers of the cerebellum of diabetic females. However, the distribution of amyloid-like pathology in the present study differs from that reported in previous studies, which have primarily described amyloid pathology in the cerebral cortex and hippocampus of diabetic and AD mice. Several factors, including differences in age, sex, and the experimental diabetes model, may explain these discrepancies [59,68]. These factors may influence the extent, distribution, or detectability of amyloid-like pathology in the brains of female diabetic mice.

4.3. Effect of Metformin on Brain Levels of Tau Protein

One of the most striking findings of the present study was the significant increase in total tau (t-tau) and phosphorylated tau (p-tau) at serine 199 (pS199) with the highest dose of metformin (250 mg/kg). The p-tau/t-tau ratio exhibited a similar pattern. Despite the favorable behavioral outcomes observed at this dose, this finding cannot be dismissed. Phosphorylation at serine 199 is a pathologically relevant tau epitope that appears in the early stages of Alzheimer's disease and other tauopathies. Hyperphosphorylated tau loses its ability to bind to microtubules, mislocalizes to the somatodendritic compartment, and adopts a β-sheet-rich conformation that promotes the formation of neurofibrillary tangles [69–71]. Ultimately, this contributes to synaptic loss and neuronal death. These changes correlate more strongly with cognitive decline than amyloid burden [72].

The pro-tauopathic effect observed at 250 mg/kg is consistent with the previously reported paradoxical effects of metformin on tau biology. In the P301S transgenic tauopathy model, chronic metformin administration increased insoluble tau species and β-sheet aggregates, despite reducing tau phosphorylation. This suggests that metformin's pro-aggregation effects can override its dephosphorylating action [73]. Conversely, in a diabetic, obese male mouse model, a 200 mg/kg i.p. dose of metformin reduced hyperphosphorylated tau through AMPK-dependent autophagic clearance [74]. Together, these findings reinforce the possibility that metformin's effects on tau are highly dose-dependent and may vary according to the experimental model and treatment conditions.

The distinct biological responses observed across metformin doses may reflect differences in metformin exposure in the brain. Pharmacokinetic evidence suggests that

higher doses of metformin do not necessarily result in proportionally higher concentrations in the brain. For example, the 150 mg/kg dose has been reported to produce a higher concentration of metformin in the cerebellum (17.1 nmol/g) than the 300 mg/kg dose (7.8 nmol/g) [36]. This finding suggests that the relationship between systemic dose and regional brain exposure may be nonlinear and could contribute to the divergent biological responses observed at different doses in the present study. Consistent with this possibility, several studies have reported that doses above 200 mg/kg may produce adverse neuronal or cognitive effects [73,75,76]. However, because tau was assessed in whole-brain homogenates, this finding cannot be directly linked to regional differences in metformin concentration.

4.4. Limitations of the Study

Several limitations of the present study should be considered. First, the estrous cycles of the female mice were not synchronized, which may have introduced variability into the behavioral and biochemical measurements. Second, although the streptozotocin-nicotinamide protocol reliably induces hyperglycemia and reproduces some metabolic features of T2DM, it does not fully capture the pathophysiological complexity of human T2DM, including progressive insulin resistance and obesity. Future studies using genetic and diet-induced models of diabetes may help determine whether these findings are also observed in models that more closely reproduce these features.

For the neuropathological assessment, brain regions were identified using anatomical landmarks instead of stereotaxic coordinates. The histological evaluation focused on the CA1 region of the hippocampus, the cerebral cortex, and the cerebellum. However, the evaluation was limited to hematoxylin and eosin and Congo red staining. Regions potentially affected by diabetes, such as the amygdala and striatum, were not examined. Consequently, the overall extent of neuronal damage and the potential effects of metformin may have been underestimated. Additionally, since the histological and biochemical assessments were performed only at the end of the 28-day treatment, temporal changes in these parameters could not be evaluated. This limits the ability to draw conclusions about their progression over time.

The lack of direct measurements of AMPK and IDE activity, as well as oxidative stress and neuroinflammatory markers, limits the interpretation of the molecular pathways underlying the effects of metformin. Additionally, the present study did not include male diabetic mice. Therefore, these findings should not be interpreted as evidence of sex-specific effects. Rather, the findings describe the metabolic and neurobehavioral effects of metformin in a female model of impaired recognition memory associated with diabetes. Direct comparisons between male and female diabetic animals are necessary to determine whether sex-dependent differences exist in the response to metformin.

Finally, cognitive function was assessed exclusively using the NORT, which limits the generalizability of the findings to other cognitive domains, such as spatial memory, working memory, and executive function. The behavioral and histological findings provide complementary evidence of the effects of diabetes and metformin treatment. However, the present study does not allow us to determine how individual brain regions contribute to recognition memory performance. Additionally, diabetes-associated visual impairment may be a confounding factor in the NORT. Future studies that incorporate additional behavioral paradigms (e.g., the Y-maze, Morris water maze, and fear conditioning) together with appropriate visual assessments would clarify whether the observed effects of metformin extend to other cognitive domains.

5. Conclusions

Subchronic metformin treatment at doses of 50, 150, and 250 mg/kg reduced hyperglycemia and improved recognition memory in female diabetic mice. Metformin normalized serum and brain insulin levels, reduced serum cholesterol at 150 and 250 mg/kg, and mitigated neuronal damage in the CA1 region of the hippocampus, cerebral cortex, and cerebellum. Metformin also reduced cerebellar Congo red-positive amyloid-like deposits and decreased insoluble $A\beta_{42}$ levels in whole-brain homogenates. However, the highest dose (250 mg/kg) increased total and phosphorylated tau protein levels in brain tissue, though it improved recognition memory. These results suggest that metformin produces beneficial metabolic, behavioral, and neuropathological changes in this female diabetic mouse model. Nevertheless, the increase in tau-related markers at the highest dose underscores the need for further research on metformin's effects on the female diabetic brain.

Author Contributions: Conceptualization, L.E.C.-P.; methodology, J.P., H.A.-M. and M.d.C.R.-S.; software, J.P.; validation, L.E.C.-P. and H.A.-M.; formal analysis, J.P., L.E.C.-P. and M.d.C.R.-S.; investigation, J.P., L.E.C.-P. and H.A.-M.; writing—original draft preparation, J.P. and L.E.C.-P.; writing—review and editing, L.E.C.-P., H.A.-M. and M.d.C.R.-S.; visualization, L.E.C.-P.; supervision, L.E.C.-P.; project administration, L.E.C.-P.; funding acquisition, L.E.C.-P. All authors have read and agreed to the published version of the manuscript.

Funding: This research received no external funding.

Institutional Review Board Statement: The animal study protocol was approved by the Ethics Committee of the Faculty of Chemical Sciences of the Autonomous University of Coahuila (TMCB-22-09-23-2 approved on 22 September 2023).

Data Availability Statement: The raw data supporting the conclusions of this article will be made available by the authors on request.

Acknowledgments: JP would like to thank the SECIHTI-Mexico scholarship program.

Conflicts of Interest: The authors declare no conflicts of interest.

Abbreviations

The following abbreviations are used in this manuscript:

T2DM	Type 2 diabetes mellitus
AD	Alzheimer's disease
DACI	Diabetes-associated cognitive impairment
CNS	Central nervous system
BBB	Blood–brain barrier
Aβ	β-amyloid
AMPK	AMP-activated protein kinase
STZ	streptozotocin
NORT	Novel Object Recognition Test
PBS	Phosphate-buffered saline
ANOVA	Analysis of variance
CA	Cornu Ammonis
ELISA	Enzyme-Linked Immunosorbent Assay
AEBSF	4-(2-aminoethyl)benzenesulfonyl fluoride hydrochloride
HRP	Horseradish peroxidase
TMB	3,3′,5,5′-Tetramethylbenzidine

References

1. Khan, M.A.B.; Hashim, M.J.; King, J.K.; Govender, R.D.; Mustafa, H.; Al Kaabi, J. Epidemiology of Type 2 Diabetes—Global Burden of Disease and Forecasted Trends. *J. Epidemiol. Glob. Health* **2020**, *10*, 107–111. [CrossRef] [PubMed]
2. Lu, X.; Xie, Q.; Pan, X.; Zhang, R.; Zhang, X.; Peng, G.; Zhang, Y.; Shen, S.; Tong, N. Type 2 diabetes mellitus in adults: Pathogenesis, prevention and therapy. *Signal Transduc. Target. Ther.* **2024**, *9*, 262. [CrossRef] [PubMed]
3. Cao, F.; Yang, F.; Li, J.; Guo, W.; Zhang, C.; Gao, F.; Sun, X.; Zhou, Y.; Zhang, W. The relationship between diabetes and the dementia risk: A meta-analysis. *Diabetol. Metab. Syndr.* **2024**, *16*, 101. [CrossRef] [PubMed]
4. Cholerton, B.; Baker, L.D.; Montine, T.J.; Craft, S. Type 2 Diabetes, Cognition, and Dementia in Older Adults: Toward a Precision Health Approach. *Diabetes Spectr.* **2016**, *29*, 210–219. [CrossRef] [PubMed]
5. Hamzé, R.; Delangre, E.; Tolu, S.; Moreau, M.; Janel, N.; Bailbé, D.; Movassat, J. Type 2 Diabetes Mellitus and Alzheimer's Disease: Shared Molecular Mechanisms and Potential Common Therapeutic Targets. *Int. J. Mol. Sci.* **2022**, *23*, 15287. [CrossRef] [PubMed]
6. Kim, H.G. Cognitive dysfunctions in individuals with diabetes mellitus. *Yeungnam Univ. J. Med.* **2019**, *36*, 183–191. [CrossRef] [PubMed]
7. Yu, X.; He, H.; Wen, J.; Xu, X.; Ruan, Z.; Hu, R.; Wang, F.; Ju, H. Diabetes-related cognitive impairment: Mechanisms, symptoms, and treatments. *Open Med.* **2025**, *20*, 20241091. [CrossRef] [PubMed]
8. Zhao, Q.; Zhang, Y.; Liao, X.; Wang, W. Executive Function and Diabetes: A Clinical Neuropsychology Perspective. *Front. Psychol.* **2020**, *11*, 2112. [CrossRef] [PubMed]
9. Kalra, S.; Raizada, N. Dyslipidemia in diabetes. *Indian Heart J.* **2024**, *76*, S80–S82. [CrossRef] [PubMed]
10. de Oliveira, J.; Engel, D.F.; de Paula, G.C.; dos Santos, D.B.; Lopes, J.B.; Farina, M.; Moreira, E.L.G.; de Bem, A.F. High Cholesterol Diet Exacerbates Blood-Brain Barrier Disruption in LDLr−/− Mice: Impact on Cognitive Function. *J. Alzheimers Dis.* **2020**, *78*, 97–115. [CrossRef] [PubMed]
11. Poblano, J.; Castillo-Tobías, I.; Berlanga, L.; Tamayo-Ordoñez, M.C.; del Carmen Rodríguez-Salazar, M.; Silva-Belmares, S.Y.; Aguayo-Morales, H.; Cobos-Puc, L.E. Drugs targeting APOE4 that regulate beta-amyloid aggregation in the brain: Therapeutic potential for Alzheimer's disease. *Basic Clin. Pharmacol. Toxicol.* **2024**, *135*, 237–249. [CrossRef] [PubMed]
12. Rudajev, V.; Novotny, J. Cholesterol as a key player in amyloid β-mediated toxicity in Alzheimer's disease. *Front. Mol. Neurosci.* **2022**, *15*, 937056. [CrossRef] [PubMed]
13. Rudajev, V.; Novotny, J. Cholesterol-dependent amyloid β production: Space for multifarious interactions between amyloid precursor protein, secretases, and cholesterol. *Cell Biosci.* **2023**, *13*, 171. [CrossRef] [PubMed]
14. Lizarbe, B.; Soares, A.F.; Larsson, S.; Duarte, J.M.N. Neurochemical Modifications in the Hippocampus, Cortex and Hypothalamus of Mice Exposed to Long-Term High-Fat Diet. *Front. Neurosci.* **2019**, *12*, 985. [CrossRef] [PubMed]
15. Parihar, M.S.; Chaudhary, M.; Shetty, R.; Hemnani, T. Susceptibility of hippocampus and cerebral cortex to oxidative damage in streptozotocin treated mice: Prevention by extracts of Withania somnifera and Aloe vera. *J. Clin. Neurosci.* **2004**, *11*, 397–402. [CrossRef] [PubMed]
16. Xiang, Q.; Tao, J.-S.; Dong, S.; Liu, X.-L.; Yang, L.; Liu, L.-N.; Deng, J.; Li, X.-H. Heterogeneity and synaptic plasticity analysis of hippocampus based on db-/- mice induced diabetic encephalopathy. *Psychoneuroendocrinology* **2024**, *159*, 106412. [CrossRef] [PubMed]
17. Lee, S.G.; Yoo, D.Y.; Jung, H.Y.; Nam, S.M.; Kim, J.W.; Choi, J.H.; Yi, S.S.; Won, M.H.; Yoon, Y.S.; Hwang, I.K.; et al. Neurons in the hippocampal CA1 region, but not the dentate gyrus, are susceptible to oxidative stress in rats with streptozotocin-induced type 1 diabetes. *Neural Regen. Res.* **2015**, *10*, 451–456. [CrossRef] [PubMed]
18. Rudolph, S.; Badura, A.; Lutzu, S.; Pathak, S.S.; Thieme, A.; Verpeut, J.L.; Wagner, M.J.; Yang, Y.-M.; Fioravante, D. Cognitive-Affective Functions of the Cerebellum. *J. Neurosci.* **2023**, *43*, 7554–7564. [CrossRef] [PubMed]
19. Zhang, P.; Duan, L.; Ou, Y.; Ling, Q.; Cao, L.; Qian, H.; Zhang, J.; Wang, J.; Yuan, X. The cerebellum and cognitive neural networks. *Front. Hum. Neurosci.* **2023**, *17*, 1197459. [CrossRef] [PubMed]
20. Atabi, F.; Moassesfar, M.; Nakhaie, T.; Bagherian, M.; Hosseinpour, N.; Hashemi, M. A systematic review on type 3 diabetes: Bridging the gap between metabolic dysfunction and Alzheimer's disease. *Diabetol. Metab. Syndr.* **2025**, *17*, 356. [CrossRef] [PubMed]
21. Sebastian, M.J.; Khan, S.K.; Pappachan, J.M.; Jeeyavudeen, M.S. Diabetes and cognitive function: An evidence-based current perspective. *World J. Diabetes* **2023**, *14*, 92–109. [CrossRef] [PubMed]
22. Dutta, S.; Shah, R.B.; Singhal, S.; Dutta, S.B.; Bansal, S.; Sinha, S.; Haque, M. Metformin: A Review of Potential Mechanism and Therapeutic Utility Beyond Diabetes. *Drug Des. Devel. Ther.* **2023**, *17*, 1907–1932. [CrossRef] [PubMed]
23. Foretz, M.; Guigas, B.; Viollet, B. Metformin: Update on mechanisms of action and repurposing potential. *Nat. Rev. Endocrinol.* **2023**, *19*, 460–476. [CrossRef] [PubMed]
24. Hurtado-Carneiro, V.; LeBaut-Ayuso, Y.; Velázquez, E.; Flores-Lamas, C.; Fernández-de la Rosa, R.; García-García, L.; Gómez-Oliver, F.; Ruiz-Albusac, J.M.; Pozo, M.Á. Effects of chronic treatment with metformin on brain glucose hypometabolism and central insulin actions in transgenic mice with tauopathy. *Heliyon* **2024**, *10*, e35752. [CrossRef] [PubMed]

25. Reed, S.; Taka, E.; Darling-Reed, S.; Soliman, K.F.A. Neuroprotective Effects of Metformin Through the Modulation of Neuroinflammation and Oxidative Stress. *Cells* **2025**, *14*, 1064. [CrossRef] [PubMed]
26. Rotermund, C.; Machetanz, G.; Fitzgerald, J.C. The Therapeutic Potential of Metformin in Neurodegenerative Diseases. *Front. Endocrinol.* **2018**, *9*, 400. [CrossRef] [PubMed]
27. Chen, Y.; Zhao, S.; Fan, Z.; Li, Z.; Zhu, Y.; Shen, T.; Li, K.; Yan, Y.; Tian, J.; Liu, Z.; et al. Metformin attenuates plaque-associated tau pathology and reduces amyloid-β burden in APP/PS1 mice. *Alzheimers Res. Ther.* **2021**, *13*, 40. [CrossRef] [PubMed]
28. Oliveira, W.H.; Braga, C.F.; Lós, D.B.; Araújo, S.M.R.; França, M.R.; Duarte-Silva, E.; Rodrigues, G.B.; Rocha, S.W.S.; Peixoto, C.A. Metformin prevents p-tau and amyloid plaque deposition and memory impairment in diabetic mice. *Exp. Brain Res.* **2021**, *239*, 2821–2839. [CrossRef] [PubMed]
29. Chen, Y.; Zhou, K.; Wang, R.; Liu, Y.; Kwak, Y.-D.; Ma, T.; Thompson, R.C.; Zhao, Y.; Smith, L.; Gasparini, L.; et al. Antidiabetic drug metformin (Glucophage^{R}) increases biogenesis of Alzheimer's amyloid peptides via up-regulating *BACE1* transcription. *Proc. Natl. Acad. Sci. USA* **2009**, *106*, 3907–3912. [CrossRef] [PubMed]
30. Chatterjee, S.; Peters, S.A.; Woodward, M.; Mejia Arango, S.; Batty, G.D.; Beckett, N.; Beiser, A.; Borenstein, A.R.; Crane, P.K.; Haan, M.; et al. Type 2 Diabetes as a Risk Factor for Dementia in Women Compared With Men: A Pooled Analysis of 2.3 Million People Comprising More Than 100,000 Cases of Dementia. *Diabetes Care* **2016**, *39*, 300–307. [CrossRef] [PubMed]
31. Verhagen, C.; Janssen, J.; Biessels, G.J.; Johansen, O.E.; Exalto, L.G. Females with type 2 diabetes are at higher risk for accelerated cognitive decline than males: CAROLINA-COGNITION study. *Nutr. Metab. Cardiovasc. Dis.* **2022**, *32*, 355–364. [CrossRef] [PubMed]
32. O'Neal, M.A. Women and the risk of Alzheimer's disease. *Front. Glob. Womens Health* **2023**, *4*, 1324522. [CrossRef] [PubMed]
33. Udeh-Momoh, C.; Watermeyer, T. Female specific risk factors for the development of Alzheimer's disease neuropathology and cognitive impairment: Call for a precision medicine approach. *Ageing Res. Rev.* **2021**, *71*, 101459. [CrossRef] [PubMed]
34. Vieira, I.H.; Barros, L.M.; Baptista, C.F.; Rodrigues, D.M.; Paiva, I.M. Recommendations for Practical Use of Metformin, a Central Pharmacological Therapy in Type 2 Diabetes. *Clin. Diabetes* **2022**, *40*, 97–107. [CrossRef] [PubMed]
35. Nair, A.B.; Jacob, S. A simple practice guide for dose conversion between animals and human. *J. Basic Clin. Pharm.* **2016**, *7*, 27–31. [CrossRef] [PubMed]
36. Łabuzek, K.; Suchy, D.; Gabryel, B.; Bielecka, A.; Liber, S.; Okopień, B. Quantification of metformin by the HPLC method in brain regions, cerebrospinal fluid and plasma of rats treated with lipopolysaccharide. *Pharmacol. Rep.* **2010**, *62*, 956–965. [CrossRef] [PubMed]
37. Cobos-Puc, L.E.; Aguayo-Morales, H. Agmatine Mitigates Diabetes-Related Memory Loss in Female Mice by Targeting I_2/I_3 Imidazoline Receptors and Enhancing Brain Antioxidant Defenses. *Antioxidants* **2025**, *14*, 837. [CrossRef] [PubMed]
38. Antunes, M.; Biala, G. The novel object recognition memory: Neurobiology, test procedure, and its modifications. *Cogn. Process.* **2012**, *13*, 93–110. [CrossRef] [PubMed]
39. Wang, J.; Ohmuraya, M.; Suyama, K.; Hirota, M.; Ozaki, N.; Baba, H.; Nakagata, N.; Araki, K.; Yamamura, K.-I. Relationship of strain-dependent susceptibility to experimentally induced acute pancreatitis with regulation of Prss1 and Spink3 expression. *Lab. Investig.* **2010**, *90*, 654–664. [CrossRef] [PubMed]
40. Zhang, Q.; Tao, X.; Xia, S.; Qu, J.; Song, H.; Liu, J.; Li, H.; Shang, D. Emodin attenuated severe acute pancreatitis via the P2X ligand-gated ion channel 7/NOD-like receptor protein 3 signaling pathway. *Oncol. Rep.* **2019**, *41*, 270–278. [CrossRef] [PubMed]
41. Tong, M.; Dominguez, C.; Didsbury, J.; de la Monte, S.M. Targeting Alzheimer's Disease Neuro-Metabolic Dysfunction with a Small Molecule Nuclear Receptor Agonist (T3D-959) Reverses Disease Pathologies. *J. Alzheimers Dis. Park.* **2016**, *6*, 238.
42. El-Far, A.H.; Elghaity, M.M.; Mohamed, S.A.; Noreldin, A.E.; Elewa, Y.H.A.; Al Jaouni, S.K.; Alsenosy, A.A. Diosgenin alleviates D-galactose-induced oxidative stress in rats' brain and liver targeting aging and apoptotic marker genes. *Front. Mol. Biosci.* **2024**, *11*, 1303379. [CrossRef] [PubMed]
43. Mansouri, R.A.; Ahmed, A.M.; Alshaibi, H.F.; Fouda, W.M.; Aboubakr, E.M. Mechanistic Insights into FOLFOX-Induced Neurotoxicity and Determination of Its Concentrations via a Novel, Simultaneous HPLC Quantification Method in Brain Tissue. *Drug Des. Devel. Ther.* **2025**, *19*, 9055–9077. [CrossRef] [PubMed]
44. Fu, Q.; Wu, J.; Zhou, X.-Y.; Ji, M.-H.; Mao, Q.-H.; Li, Q.; Zong, M.-M.; Zhou, Z.-Q.; Yang, J.-J. NLRP3/Caspase-1 Pathway-Induced Pyroptosis Mediated Cognitive Deficits in a Mouse Model of Sepsis-Associated Encephalopathy. *Inflammation* **2019**, *42*, 306–318. [CrossRef] [PubMed]
45. Ghasemi, A.; Khalifi, S.; Jedi, S. Streptozotocin-nicotinamide-induced rat model of type 2 diabetes (review). *Acta Physiol. Hung.* **2014**, *101*, 408–420. [CrossRef] [PubMed]
46. Cardinal, J.W.; Allan, D.J.; Cameron, D.P. Differential metabolite accumulation may be the cause of strain differences in sensitivity to streptozotocin-induced beta cell death in inbred mice. *Endocrinology* **1998**, *139*, 2885–2891. [CrossRef]
47. Hayashi, K.; Kojima, R.; Ito, M. Strain differences in the diabetogenic activity of streptozotocin in mice. *Biol. Pharm. Bull.* **2006**, *29*, 1110–1119. [CrossRef] [PubMed]

48. Wszola, M.; Klak, M.; Kosowska, A.; Tymicki, G.; Berman, A.; Adamiok-Ostrowska, A.; Olkowska-Truchanowicz, J.; Uhrynowska-Tyszkiewicz, I.; Kaminski, A. Streptozotocin-Induced Diabetes in a Mouse Model (BALB/c) Is Not an Effective Model for Research on Transplantation Procedures in the Treatment of Type 1 Diabetes. *Biomedicines* **2021**, *9*, 1790. [CrossRef] [PubMed]
49. Chandrasekaran, P.; Weiskirchen, R. The Role of Obesity in Type 2 Diabetes Mellitus—An Overview. *Int. J. Mol. Sci.* **2024**, *25*, 1882. [CrossRef] [PubMed]
50. Kennard, M.R.; Nandi, M.; Chapple, S.; King, A.J. The glucose tolerance test in mice: Sex, drugs and protocol. *Diabetes Obes. Metab.* **2022**, *24*, 2241–2252. [CrossRef] [PubMed]
51. Matsui, Y.; Hirasawa, Y.; Sugiura, T.; Toyoshi, T.; Kyuki, K.; Ito, M. Metformin Reduces Body Weight Gain and Improves Glucose Intolerance in High-Fat Diet-Fed C57BL/6J Mice. *Biol. Pharm. Bull.* **2010**, *33*, 963–970. [CrossRef] [PubMed]
52. Ojuade, F.I.; Olorundare, O.E.; Akanbi, O.B.; Afolabi, S.O.; Njan, A.A. Antidiabetic and antihyperlipidemic effects of aqueous extract of Parquetina nigrescens in streptozotocin–nicotinamide induced type 2 diabetic rats. *Heliyon* **2021**, *7*, e07363. [CrossRef] [PubMed]
53. Xu, P.-X.; Wang, S.-W.; Yu, X.-L.; Su, Y.-J.; Wang, T.; Zhou, W.-W.; Zhang, H.; Wang, Y.-J.; Liu, R.-T. Rutin improves spatial memory in Alzheimer's disease transgenic mice by reducing Aβ oligomer level and attenuating oxidative stress and neuroinflammation. *Behav. Brain Res.* **2014**, *264*, 173–180. [CrossRef] [PubMed]
54. Rhea, E.M.; Banks, W.A.; Raber, J. Insulin Resistance in Peripheral Tissues and the Brain: A Tale of Two Sites. *Biomedicines* **2022**, *10*, 1582. [CrossRef] [PubMed]
55. Burillo, J.; Marqués, P.; Jiménez, B.; González-Blanco, C.; Benito, M.; Guillén, C. Insulin Resistance and Diabetes Mellitus in Alzheimer's Disease. *Cells* **2021**, *10*, 1236. [CrossRef] [PubMed]
56. LaMoia, T.E.; Shulman, G.I. Cellular and Molecular Mechanisms of Metformin Action. *Endocr. Rev.* **2020**, *42*, 77–96. [CrossRef] [PubMed]
57. Dutta, B.J.; Singh, S.; Seksaria, S.; Das Gupta, G.; Singh, A. Inside the diabetic brain: Insulin resistance and molecular mechanism associated with cognitive impairment and its possible therapeutic strategies. *Pharmacol. Res.* **2022**, *182*, 106358. [CrossRef] [PubMed]
58. Khaleghi-Mehr, M.; Delshad, A.-A.; Shafie-Damavandi, S.; Roghani, M. Metformin mitigates amyloid β1-40-induced cognitive decline via attenuation of oxidative/nitrosative stress and neuroinflammation. *Metab. Brain Dis.* **2023**, *38*, 1127–1142. [CrossRef] [PubMed]
59. Ou, Z.; Kong, X.; Sun, X.; He, X.; Zhang, L.; Gong, Z.; Huang, J.; Xu, B.; Long, D.; Li, J.; et al. Metformin treatment prevents amyloid plaque deposition and memory impairment in APP/PS1 mice. *Brain Behav. Immun.* **2018**, *69*, 351–363. [CrossRef] [PubMed]
60. Liu, L.-P.; Yan, T.-H.; Jiang, L.-Y.; Hu, W.; Hu, M.; Wang, C.; Zhang, Q.; Long, Y.; Wang, J.-Q.; Li, Y.-Q.; et al. Pioglitazone ameliorates memory deficits in streptozotocin-induced diabetic mice by reducing brain β-amyloid through PPARγ activation. *Acta Pharmacol. Sin.* **2013**, *34*, 455–463. [CrossRef] [PubMed]
61. Liu, Y.; Liu, H.; Yang, J.; Liu, X.; Lu, S.; Wen, T.; Xie, L.; Wang, G. Increased amyloid β-peptide (1–40) level in brain of streptozotocin-induced diabetic rats. *Neuroscience* **2008**, *153*, 796–802. [CrossRef] [PubMed]
62. Titisari, N.; Ahmad, H.; Samsulrizal, N.; Fauzi, A.; Abdul Razak, I.S. The mechanism underlying streptozotocin injection for the development of a nontransgenic Alzheimer's disease animal model. *Open Vet. J.* **2025**, *15*, 594–600. [CrossRef] [PubMed]
63. Ueno, H.; Yamaguchi, T.; Fukunaga, S.; Okada, Y.; Yano, Y.; Hoshino, M.; Matsuzaki, K. Comparison between the aggregation of human and rodent amyloid β-proteins in GM1 ganglioside clusters. *Biochemistry* **2014**, *53*, 7523–7530. [CrossRef] [PubMed]
64. Metzendorf, N.G.; Sehlin, D.; Hultqvist, G. Key considerations for ELISA-based quantification of diverse amyloid beta forms in murine brain homogenates. *Front. Neurosci.* **2025**, *19*, 1645952. [CrossRef] [PubMed]
65. Wang, J.Q.; Yin, J.; Song, Y.F.; Zhang, L.; Ren, Y.X.; Wang, D.G.; Gao, L.P.; Jing, Y.H. Brain aging and AD-like pathology in streptozotocin-induced diabetic rats. *J. Diabetes Res.* **2014**, *2014*, 796840. [CrossRef] [PubMed]
66. Wu, C.; Scott, J.; Shea, J.E. Binding of Congo red to amyloid protofibrils of the Alzheimer Aβ(9-40) peptide probed by molecular dynamics simulations. *Biophys. J.* **2012**, *103*, 550–557. [CrossRef] [PubMed]
67. Lu, X.Y.; Huang, S.; Chen, Q.B.; Zhang, D.; Li, W.; Ao, R.; Leung, F.C.; Zhang, Z.; Huang, J.; Tang, Y.; et al. Metformin Ameliorates Aβ Pathology by Insulin-Degrading Enzyme in a Transgenic Mouse Model of Alzheimer's Disease. *Oxid. Med. Cell. Longev.* **2020**, *2020*, 2315106. [CrossRef] [PubMed]
68. Carvalho, C.; Machado, N.; Mota, P.C.; Correia, S.C.; Cardoso, S.; Santos, R.X.; Santos, M.S.; Oliveira, C.R.; Moreira, P.I. Type 2 Diabetic and Alzheimer's Disease Mice Present Similar Behavioral, Cognitive, and Vascular Anomalies. *J. Alzheimers Dis.* **2013**, *35*, 623–635. [CrossRef] [PubMed]
69. Bakota, L.; Tulva, K.; Trushina, N.I.; Brandt, R. Beyond microtubule regulation: The multifaceted roles of tau in neuronal function and dysfunction. *Transl. Psychiatry* **2026**, *16*, 223. [CrossRef] [PubMed]
70. Lane-Donovan, C.; Smith, A.W.; Saloner, R.; Miller, B.L.; Casaletto, K.B.; Kao, A.W. Tau phosphorylation at Alzheimer's disease biomarker sites impairs its cleavage by lysosomal proteases. *Alzheimers Dement.* **2025**, *21*, e70320. [CrossRef] [PubMed]

71. Luna-Viramontes, N.I.; Campa-Córdoba, B.B.; Ontiveros-Torres, M.; Harrington, C.R.; Villanueva-Fierro, I.; Guadarrama-Ortíz, P.; Garcés-Ramírez, L.; de la Cruz, F.; Hernandes-Alejandro, M.; Martínez-Robles, S.; et al. PHF-Core Tau as the Potential Initiating Event for Tau Pathology in Alzheimer's Disease. *Front. Cell. Neurosci.* **2020**, *14*, 247. [CrossRef] [PubMed]
72. Avila, J.; Lucas, J.J.; Pérez, M.; Hernández, F. Role of Tau Protein in Both Physiological and Pathological Conditions. *Physiol. Rev.* **2004**, *84*, 361–384. [CrossRef] [PubMed]
73. Barini, E.; Antico, O.; Zhao, Y.; Asta, F.; Tucci, V.; Catelani, T.; Marotta, R.; Xu, H.; Gasparini, L. Metformin promotes tau aggregation and exacerbates abnormal behavior in a mouse model of tauopathy. *Mol. Neurodegener.* **2016**, *11*, 16. [CrossRef] [PubMed]
74. Chen, J.-L.; Luo, C.; Pu, D.; Zhang, G.-Q.; Zhao, Y.-X.; Sun, Y.; Zhao, K.-X.; Liao, Z.-Y.; Lv, A.-K.; Zhu, S.-Y.; et al. Metformin attenuates diabetes-induced tau hyperphosphorylation in vitro and in vivo by enhancing autophagic clearance. *Exp. Neurol.* **2019**, *311*, 44–56. [CrossRef] [PubMed]
75. Liu, D.; Cao, H.; Baranova, A.; Xu, C.; Zhang, F. Opposite causal effects of type 2 diabetes and metformin on Alzheimer's disease. *J. Prev. Alzheimers Dis.* **2025**, *12*, 100129. [CrossRef] [PubMed]
76. Li, W.; Chaudhari, K.; Shetty, R.; Winters, A.; Gao, X.; Hu, Z.; Ge, W.P.; Sumien, N.; Forster, M.; Liu, R.; et al. Metformin Alters Locomotor and Cognitive Function and Brain Metabolism in Normoglycemic Mice. *Aging Dis.* **2019**, *10*, 949–963. [CrossRef] [PubMed]

Disclaimer/Publisher's Note: The statements, opinions and data contained in all publications are solely those of the individual author(s) and contributor(s) and not of MDPI and/or the editor(s). MDPI and/or the editor(s) disclaim responsibility for any injury to people or property resulting from any ideas, methods, instructions or products referred to in the content.